Inorganic Chemistry

Article

pubs.acs.org/IC

# Picolinate-Containing Macrocyclic $Mn^{2+}$ Complexes as Potential MRI Contrast Agents

Enikő Molnár,[‖] Nathalie Camus,[§] Véronique Patinec,[§] Gabriele A. Rolla,[‡] Mauro Botta,[‡] Gyula Tircsó,*[,‖] Ferenc K. Kálmán,[‖] Tamás Fodor,[‖] Raphaël Tripier,*[,§] and Carlos Platas-Iglesias*[,†]

[†]Departamento de Química Fundamental, Facultade de Ciencias, Universidade da Coruña, Campus da Zapateira-Rúa da Fraga 10, 15008 A Coruña, Spain

[‡]Dipartimento di Scienze e Innovazione Tecnologica, Università del Piemonte Orientale "Amedeo Avogadro", Viale T. Michel 11, 15121 Alessandria, Italy

[§]Université de Bretagne Occidentale, UMR-CNRS 6521, UFR des Sciences et Techniques, 6 avenue Victor le Gorgeu, C.S. 93837, 29238 BREST Cedex 3, France

[‖]Department of Inorganic and Analytical Chemistry, Faculty of Science and Technology, University of Debrecen, Egyetem tér 1, H-4032 Debrecen, Hungary

Supporting Information

**ABSTRACT:** We report the synthesis of the ligand Hnompa (6-((1,4,7-triazacyclononan-1-yl)methyl)picolinic acid) and a detailed characterization of the $Mn^{2+}$ complexes formed by this ligand and the related ligands Hdompa (6-((1,4,7,10-tetraazacyclododecan-1-yl)methyl)picolinic acid) and Htempa (6-((1,4,8,11-tetraazacyclotetradecan-1-yl)methyl)-picolinic acid). These ligands form thermodynamically stable complexes in aqueous solution with stability constants of $\log K_{MnL}$ = 10.28(1) (nompa), 14.48(1) (dompa), and 12.53(1) (tempa). A detailed study of the dissociation kinetics of these $Mn^{2+}$ complexes indicates that the decomplexation reaction at about neutral pH occurs mainly following a spontaneous dissociation mechanism. The X-ray structure of $[Mn_2(nompa)_2(H_2O)_2](ClO_4)_2$ shows that the $Mn^{2+}$ ion is seven-coordinate in the solid state, being directly bound to five donor atoms of the ligand, the oxygen atom of a coordinated water molecule and an oxygen atom of a neighboring $nompa^-$ ligand acting as a bridging bidentate carboxylate group ($\mu$–$\eta^1$-carboxylate). Nuclear magnetic relaxation dispersion ($^1$H NMRD) profiles and $^{17}$O NMR chemical shifts and transverse relaxation rates of aqueous solutions of $[Mn(nompa)]^+$ indicate that the $Mn^{2+}$ ion is six-coordinate in solution by the pentadentate ligand and one inner-sphere water molecule. The analysis of the $^1$H NMRD and $^{17}$O NMR data provides a very high water exchange rate of the inner-sphere water molecule ($k_{ex}^{298} = 2.8 \times 10^9$ s$^{-1}$) and an unusually high value of the $^{17}$O hyperfine coupling constant of the coordinated water molecule ($A_O/\hbar = 73.3 \pm 0.6$ rad s$^{-1}$). DFT calculations performed on the $[Mn(nompa)(H_2O)]^+ \cdot 2H_2O$ system (TPSSh model) provide a $A_O/\hbar$ value in excellent agreement with the one obtained experimentally.

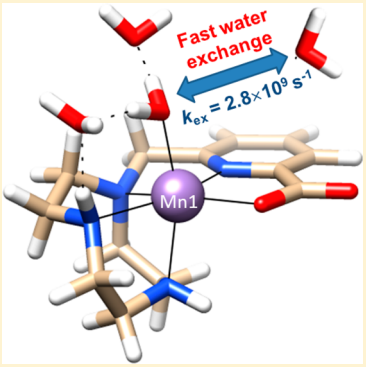


## INTRODUCTION

Magnetic resonance imaging (MRI) is a diagnostic technique widely used in radiology to obtain detailed images of the body. The so-called contrast agents (CAs) are paramagnetic compounds that increase the contrast between the specific tissue or organ of interest and the surrounding tissues of the body. Most of the compounds that entered into clinical practice as CAs are $Gd^{3+}$ complexes of poly(aminocarboxylate) ligands. However, a disease called nephrogenic systemic fibrosis (NSF) associated with the release of toxic $Gd^{3+}$ from $Gd^{3+}$-based CAs in patients suffering from severe renal failure has renewed interest in the design, synthesis, and studies of new ligands, with improved equilibrium and kinetic properties for $Ln^{3+}$ ion complexation. Alternatively, large efforts have been devoted to find less toxic CA candidates based on endogenous metal ions. Indeed, increasing attention has been devoted recently to $Mn^{2+}$ complexes of certain macrocyclic polyamines and their acetate, phosphonate, or phosphinate derivatives as possible substitutes for $Gd^{3+}$ complexes.[1] In this respect, although the complexes of $Mn^{2+}$ ion that incorporate at least one water molecule in the inner coordination sphere are the most promising ones, some $Fe^{2+}$-ion-based complexes were also found to display favorable properties as possible paramagnetic chemical exchange saturation transfer agents (ParaCEST).[2] More recently, these studies were extended further, and $Ni^{2+}$ and $Co^{2+}/Co^{3+}$ complexes were also investigated as possible ParaCEST agents,[3] but clearly the $Mn^{2+}$ cation has the greatest potential as far as possible substitutes for the $Gd^{3+}$-based agents are concerned.

Historically, the $Mn^{2+}$ ion played an important role in the development of MRI as it was among the first studied as a $T_1$ shortening agent by examining the binding of paramagnetic

Received: January 29, 2014
Published: April 28, 2014

   dx.doi.org/10.1021/ic500231z | Inorg. Chem. 2014, 53, 5136–5149

**Chart 1. Ligands Used for $Mn^{2+}$ Complexation**

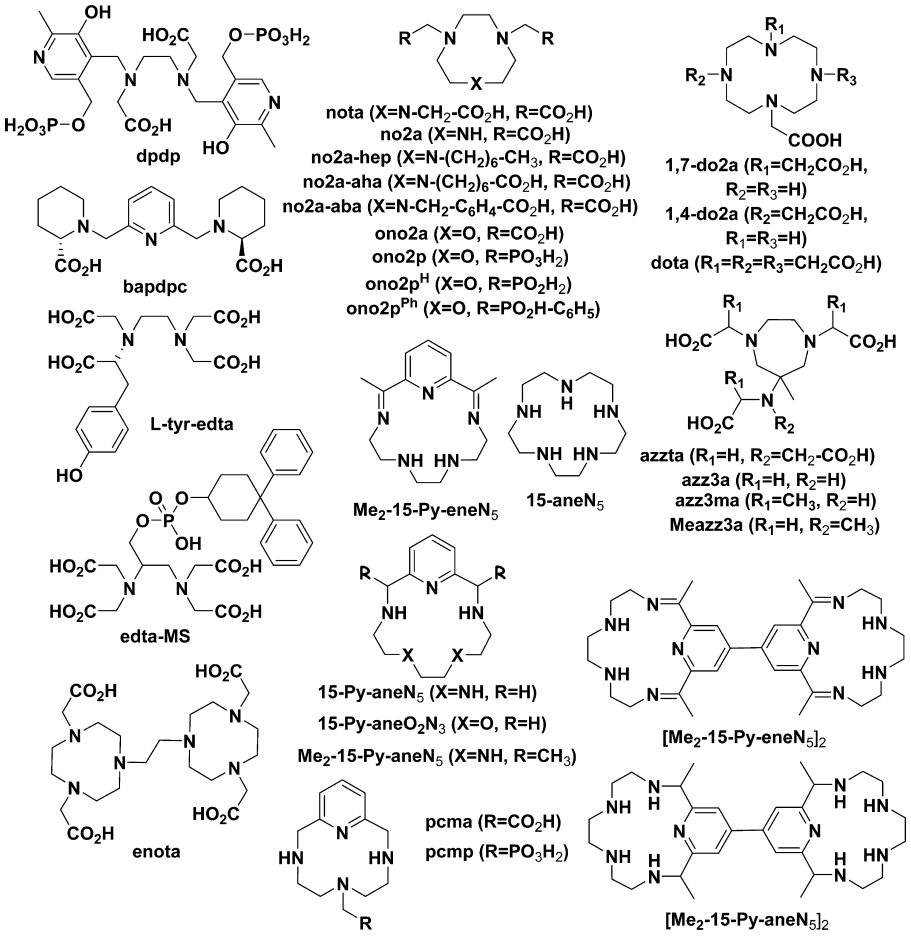


transition metal ions to DNA.[4] More than 10 years later, Lauterbur used a $MnSO_4$ solution to describe the 3D imaging technique known today as MRI.[5] Although the water exchange rates of $Mn^{2+}$ complexes formed with open-chain ligands (e.g., edta, phdta) were described relatively early,[6] the far-from-optimal physicochemical properties of these complexes and much better relaxation properties of the $Gd^{3+}$ ion and its chelates caused nearly all $Mn^{2+}$ agents to vanish from the field of MRI. The only $Mn^{2+}$-based complex that survived for a while was $[Mn(dpdp)]^{4-}$ (Chart 1), in which the relaxation enhancement arises from $Mn^{2+}$ released from the complex in vivo (manganese-enhanced magnetic resonance imaging − MEMRI).[7] However, at the elevated concentrations typically used for MRI (0,05−0,10 mmol/kg of body weight) the release of $Mn^{2+}$ results in its accumulation in the brain, which causes neurotoxicity leading to a syndrome known as "mangansim" with Parkinson-like symptoms.[8]

Owing to the increasing importance of the $Mn^{2+}$ complexes in the past 4−5 years, large efforts were devoted to find an appropriate ligand by balancing between contradictory requirements (i.e., thermodynamic stability and kinetic inertness vs low ligand denticity enabling water molecule(s) to be coordinated in its $Mn^{2+}$ complexes), most of them being macrocyclic pyridine-based ligands or derivatives of the aazta ligand.[9] A report of a series of rigid pyridine-based 15−18 membered macrocyclic ligands as possible $Mn^{2+}$ binding agents for MRI applications dates back to 1992,[10] although some of the complexes summarized in the given report were previously prepared or characterized in the solid state.[11] Tóth and co-workers have returned to this class of ligands more recently and determined protonation constants of the ligands, stabilities of the complexes, solvent exchange and decomplexation kinetics, and structural properties of two members of the given ligand class (15-Py-aneN$_5$ and 15-Py-aneO$_2$N$_3$).[12] The complexes were found to be thermodynamically stable with relaxivities similar to those of typical low-molecular-weight $Gd^{3+}$ chelates. However, the relatively low kinetic inertness of the studied complexes along with the excellent SOD mimics does not allow the application of these complexes in vivo. Ivanović-Burmazović and co-workers extended the idea and synthesized Me2-Py-ene- and Me2-Py-ane-based ligands capable of binding two $Mn^{2+}$ ions simultaneously and studied their dinuclear $Mn^{2+}$ complexes in solution and solid state.[13] Although the relaxivities of the $Mn^{2+}$ complexes were not reported, other physicochemical parameters (stability, water exchange rate) were found to be similar to those of monomeric complexes, which indicates the absence of interactions between the two paramagnetic centers. The dimeric triazacyclononane-based ligand $H_4$enota was also examined with an aim to bind $Mn^{2+}$ ion for MRI applications.[14] The results of equilibrium, solvent exchange kinetics, and structural characterization studies indicated a high stable $Mn^{2+}$ complex with one water molecule coordinated to each metal center that is slightly more labile than in the aqua ion ($k_{ex}^{298} = 5.5 \times 10^7$ s$^{-1}$ vs $2.8 \times 10^7$ s$^{-1}$).[15] In spite of the very promising data, a recent report highlighted that $Mn^{2+}$ complexes formed with no2a derivative ligands (no2a and


dx.doi.org/10.1021/ic500231z | Inorg. Chem. 2014, 53, 5136−5149

ono2a) are kinetically labile and may lose the $Mn^{2+}$ ion in highly competitive biological fluids.[16] The 12-membered pyridine-containing macrocyclic ligands bearing one acetate or phosphonate pendant arms (pcma and pcmp) were also synthesized and explored by the same group as possible $Mn^{2+}$-binding agents.[17] These ligands possess five possible donor atoms, and the sixth coordination site in their $Mn^{2+}$ complexes is occupied by a water molecule that exchanges extremely rapidly with the bulk water, as evidenced by $^{17}O$ NMR studies. These ligands were found to form thermodynamically stable complexes with $Mn^{2+}$, but owing to the low kinetic inertness and air-sensitivity, their application as CAs in MRI cannot be recommended. The 12-membered hexadentate macrocyclic ligands 1,4-do2a and 1,7-do2a were also shown to form thermodynamically stable $Mn^{2+}$ complexes in aqueous solutions, but only the 1,4-do2a complex contained a coordinated water molecule.[18]

Among the open-chain ligands cdta is the only one that forms a thermodynamically stable and kinetically satisfactory (inert) $Mn^{2+}$ complex with a relatively high relaxivity and acceptable redox stability.[19] Besides the traditional CA research, $Mn^{2+}$ complexes have diffused into the smart CA research: redox-sensitive agents,[20] as well as agents capable of binding to serum proteins, thus enabling high-resolution imaging of blood vessels in vivo, were designed and reported.[21] The ligands used for $Mn^{2+}$ ion complexation in these reports were either dtpa, rigidified edta, or 2,6-bis(aminomethyl)pyridine derivatives.[19−22] All of these examples indicate that the rigidified pyridine unit (present mostly in the macrocycle) is a highly favored building block when designing ligands for $Mn^{2+}$ ion encapsulation. However, little is known about the effect of the pyridine unit (2-pyridinecarboxylate = picolinate) on the thermodynamic and kinetic (water exchange and dissociation kinetics) properties of the $Mn^{2+}$ complexes when one is attached to the macrocycle as a pendant arm. A previous report was devoted to the synthesis and study of the complexation behavior of two (cyclen- and cyclam-based) monopicolinates (Hdompa and Htempa, Chart 2) with $Cu^{2+}$ and $Zn^{2+}$ ions.[23]

**Chart 2. Ligands Investigated in This Work**

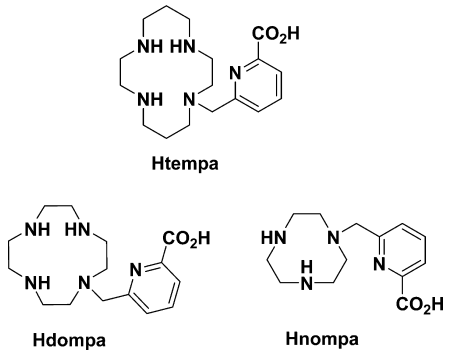


The acid−base properties of these ligands as well as the stability constants of their complexes formed with $Cu^{2+}$ and $Zn^{2+}$ were investigated in solution (stability, kinetics of decomplexation, CV and EPR spectroscopy) and in solid state (X-ray diffraction studies). Furthermore, these ligands were also shown to present an attractive behavior in vivo when radiolabeled with $^{64}Cu$.[24] In this paper, we present the results of the synthesis of the nine-membered monopicolinate derivative ligand Hnompa and equilibrium studies performed on the $Mn^{2+}$ complexes of nompa, dompa, and tempa ligands (Chart 2). Because the $Cu^{2+}$ ion was used as a ligand scavenger in the decomplexation reactions of $[Mn(nompa)]^+$ and $[Mn(dompa)]^+$ complexes, the stability of the $[Cu(nompa)]^+$ and $[Cu(dompa)]^+$ were also determined by using UV−vis spectrophotometry. The water exchange rate of the $[Mn(nompa)(H_2O)]^+$ complex and its efficiency as a potential MRI contrast agent was also assessed by means of $^{17}O$ NMR and $^1H$ NMRD measurements. The structure of $[Mn(nompa)]^+$ in the solid state was determined by single-crystal X-ray diffraction studies.

## EXPERIMENTAL AND COMPUTATIONAL SECTION

**Materials and Methods.** Reagents were purchased from ACROS Organics and from Aldrich Chemical Co. The reagents 1,4,7-triazacyclononane (tacn), cyclen and cyclam were purchased from CheMatech (Dijon, France). Acetonitrile, tetrahydrofuran, toluene, and dichloromethane were distilled before use. Elemental analyses were performed at the Institut des Sciences Analytiques, CNRS, 69100 Villeurbanne, or at the Service de Microanalyse, CNRS, 91198 Gif sur Yvette, France. NMR and MALDI mass spectra were recorded at the "Services Communs" of the University of Brest. $^1H$ and $^{13}C$ NMR spectra were recorded with a Bruker AMX-3 300 (300 MHz for $^1H$) spectrometer, and MALDI mass spectra were recorded with an Autoflex MALDI TOF III LRF200 CID spectrometer. Ligands Hdompa and Htempa[23] and 6-chloromethylpyridine-2-carboxylic acid methyl ester[25] were synthesized according to published methods.

**6-((1,4,7-Triazacyclononan-1-yl)methyl)picolinic acid (Hnompa).** *N*-Dimethoxymethyl-*N*,*N*-dimethylamine (572 mg, 4.8 mmol, 1.1 equiv) was added to a solution of tacn (560 mg, 4.34 mmol) in toluene (15 mL). The solution was stirred at room temperature for 12 h. The solvent was then evaporated under reduced pressure to yield intermediate **2** as an oily product (580 mg, 4.16 mmol, yield 96%). NMR ($CDCl_3$) $^1H$ 2.36 (m, 6H, $CH_2$) 2.63 (m, 6H, $CH_2$) 4.57 (s, 1H, *CH*); $^{13}C\{^1H\}$ 51.3 ($CH_2$) 103.6 (*CH*). A 850 mg amount of 6-chloromethylpyridine-2-carboxylic acid methyl ester (compound **3**, 4.6 mmol, 1.1 equiv) dissolved in 10 mL of freshly distilled THF was added to the previous crude product dissolved in 2 mL of distilled $CH_2Cl_2$. The mixture was stirred at room temperature for 8 days, and the white solid precipitated was filtered, washed with THF and dried under vacuum to give 860 mg of compound **4** (yield 63%). Hydrolysis of the orthoamide function of **4** occurred partially in $D_2O$ in the NMR tube giving a mixture of **4** and its formamide form characterized by the following different peaks: **4**: $^1H$ NMR ($D_2O$, 300 MHz): 2.87−2.96 (m), 3.04−3.10 (m), 3.12−3.38 (m), 3.50−3.62 (m), 3.75−3.80 (m), 3.99 (s), 4.00 (s), 4.17 (s), 4.13−4.08 (m), 4.80 (s, $CH_{2\text{picolinate}}$), 6.06 (s, *CH*), 7.54 (d), 7.65 (m), 7.71 (s), 8.06 (d), 8.18 (t), 8.28 (d) ($C_5H_3N$); $^{13}C\{^1H\}$ NMR ($D_2O$, 75 MHz): 54.2 ($CH_{2\ tacn}$), 56.2 ($CH_3$), 57.3, 61.1 ($CH_{2\ tacn}$), 64.7 ($CH_{2\ picolinate}$), 122.7 (*CH*), 129.2, 133.6, 142.9 ($CH_{picolinate}$), 150.4, 152.4 ($C_{picolinate}$), 169.1 (CO) ; formamide (2 rotamers): 44.4, 46.1, 46.2, 47.6, 47.7, 47.9, 48.9, 49.7, 51.7, 52.7, 53.2, 54.5, 54.8 ($CH_{2\ tacn}$), 56.0, 56.1 ($CH_3$), 60.4, 61.4 ($CH_{2\ picolinate}$), 127.1, 129.6, 129.7, 141.7, 141.8 ($CH_{picolinate}$), 149.05, 149.1, 163.4 ($C_{picolinate}$), 169.0 (N-CHO), 169.5 (CO), 169.9 (N-CHO).

Compound **4** (860 mg, 2.65 mmol) was dissolved in 10 mL of a methanol/HCl 12 M (1/1) mixture and stirred while heating to reflux for 12 h. Evaporation of the aqueous solvent gave a solid that was dissolved in 3 M HCl solution (10 mL) and stirred at reflux for 12h. After cooling to room temperature, the solvent was removed under reduced pressure to give a brown powder that was dissolved in hot ethanol. Slow cooling of the ethanolic solution to room temperature gave a beige solid that corresponds to Hnompa as its hydrochloride form. The solid was isolated by filtration and dried under vacuum (770 mg, 2.41 mmol, yield 91%).

$^1H$ NMR ($D_2O$, 300 MHz): 3.15 (m, $CH_{2tacn}$, 4H), 3.33 (m, $CH_{2tacn}$, 4H), 3.80 (bs, $CH_{2tacn}$, 4H), 4.23 (s, $CH_{2picolinate}$, 2H), 7.58 (d, $CH_{picolinate}$, 1H), 8.06 (t, $CH_{picolinate}$, 1H), 8.11 (d, $CH_{picolinate}$, 1H); $^{13}C\{^1H\}$ NMR ($D_2O$, 75 MHz): 45.9, 47.4, 51.5 ($CH_{2\ tacn}$), 60.1


dx.doi.org/10.1021/ic500231z | Inorg. Chem. 2014, 53, 5136−5149

($CH_{2\ picolinate}$), 127.5, 129.9, 142.8 (CH picolinate), 149.5, 162.0 (C picolinate), 169.1 (CO). MALDI-TOF: $m/z$ 265.04 [M+1$^+$]. Anal. Calcd for $C_{13}H_{20}N_4O_2 \cdot 2.1$ HCl·0.8 $H_2O$: C, 43.95; H, 6.72; N, 15.77; Cl, 20.95. Found: C, 44.13; H, 6.38; N, 15.87; Cl, 20.58.

**Potentiometric Measurements.** The $MnCl_2$ and $CuCl_2$ stock solutions were prepared from the highest analytical grade chemicals, and their concentrations were determined by complexometric titration with standardized $Na_2H_2$edta and eriochrome black T indicator in the presence of ascorbic acid and potassium hydrogen tartrate for $MnCl_2$ and murexide indicator for the $CuCl_2$ stock solution. The concentrations of the ligand stock solutions were determined by pH-potentiometric titrations by using the data obtained in the presence and absence of a 2-fold excess of $Mn^{2+}$. For determining the protonation constants of the ligands, pH-potentiometric titrations were performed with 0.2 M NaOH, using 0.0025 M ligand solutions. The ionic strength was set to 0.15 M by using NaCl. The titrated samples (starting volume of 8 mL) were stirred mechanically and thermostated at 25 °C by using a circulating water bath (±0.1 °C). To avoid the effect of $CO_2$, $N_2$ gas was bubbled through them during the titration process. The pH-potentiometric titrations were carried out with a Metrohm 785 DMP Titrino titration workstation with the use of a Metrohm 6.0233.100 combined electrode in the pH range of 1.8−12.0. For the calibration of the pH-meter, KH-phthalate (pH = 4.005) and borax (pH = 9.177) buffers were used, and the $H^+$ concentrations were calculated from the measured pH values by applying the method proposed by Irving et al.[26] A solution of approximately 0.01 M HCl was titrated with a 0.2 M NaOH solution (0.15 M NaCl), and the difference between the measured and calculated pH values (for the samples with pH < 2.4) was used to calculate the [$H^+$] from the pH values measured in the titration experiments. The basic points of the acid−base titration (pH > 11.0) were used to calculate the ionic product of water which was found to be 13.763 under our experimental setup. For the calculation of the equilibrium constants, the PSEQUAD program was used.[27] The stability constants of the $Mn^{2+}$ complexes were determined by the direct pH-potentiometric method by titrating samples with 1:1 metal-to-ligand ratio (the number of data pairs was 146, 223, and 197 for the nompa, dompa, and tempa ligands, respectively), allowing 1 min for the sample equilibration to occur while the so-called batch method was applied for the $Cu^{2+}$ complexes by using 1 week for equilibration time. The stability constants of the $Cu^{2+}$ complexes were too high to be determined by pH-potentiometry, hence a direct UV−vis spectrophotometric method was utilized to determine the stability constants. The spectrophotometric measurements were performed with the use of a Cary 1E spectrophotometer at 25 °C, using semimicro 1.0 cm cells. The molar absorptivities of the $CuCl_2$, [Cu(nompa)]$^+$, and [Cu(Hdompa)]$^{2+}$ complexes were determined at 27 wavelengths (540−800 nm range) by recording the spectra of $2.5 \times 10^{-3}$, $5.0 \times 10^{-3}$, $7.5 \times 10^{-3}$, and $1.0 \times 10^{-2}$ M solutions. The deprotonation step of the coordinated water molecule in [Cu(nompa)]$^+$ was followed by direct pH-potentiometry by titrating the complex (0.0025 M) with a standardized NaOH solution. A pH-titration of the [Cu(dompa)]$^+$ complex was also performed under similar conditions (pH range of 1.40−12.0, $V$ = 6.0 mL, and $c_{Cu} = c_{dompa}$ = 3.0 mmol/dm$^3$). However, the deprotonation was not detected in this case, in good agreement with the UV−vis titration data. The Hdompa and Htempa ligands used in the equilibrium, kinetic and relaxometric studies were purified using HPLC on a Phenomenex Luna 5u C18(2) 100A AXIA packed reverse phase column by using water as a mobile phase ($R_t$ = 1.64 min (Hdompa) and 1.69 min (Htempa)).

**Kinetic Measurements.** The dissociation rates of [Mn(dompa)]$^+$ and [Mn(nompa)]$^+$ complexes were investigated at 25 °C and 0.15 M NaCl ionic strength by a stopped-flow method following the formation of the $Cu^{2+}$ complex at 310 nm using an Applied Photophysics DX-17MV instrument. The decomplexation reactions were carried out by using $Cu^{2+}$ ion as exchanging metal ion in the pH range of 3.67−4.65 for the dompa and 3.47−5.08 for the nompa complex. All reactions were performed under pseudo-first-order conditions, where the metal ion was in 10−40-fold excess (although no direct involvement of the metal ion in the dissociation was observed) and the concentration of the complexes was set to $2.5 \times 10^{-4}$ M. The kinetic studies were carried out by using noncoordinating buffers, $N$,$N'$-dimethylpiperazine (dmp, $\log K^2_H$ = 4.19 (0.01)) and $N'$-methylpiperazine (nmp, $\log K^2_H$ = 4.92(0.02)) at 0.05 M concentration to maintain constant pH in the samples.

**Determination of the Relaxivity of the $Mn^{2+}$ Complexes.** The relaxation times of water protons were measured at 20 MHz with a Bruker Minispec MQ-20 NMR Analyzer. The temperature of the sample holder was set (25.0 ± 0.2 °C) and controlled with the use of a circulating water bath. The longitudinal relaxation times ($T_1$) were measured by using the inversion recovery method (180° − $\tau$ − 90°) by averaging 5−6 data points obtained at 14 different $\tau$ values. The relaxivities of the complexes were determined according to a methodology slightly different from the standard one (by plotting the reciprocal longitudinal relaxation times of the complexes against their concentrations). Batch samples were prepared under argon atmosphere having the ligand present at 2.0 mM concentration (the pH in these samples was kept constant at pH = 8.08 with the use of HEPES buffer ($I$ = 0.15 M NaCl, 25 °C)). Various amounts of $MnCl_2$ were added to these solutions, and longitudinal relaxation times of the solutions were measured. Because under these conditions only one $Mn^{2+}$-ion-containing species is present in solution in each system, (nompa, dompa, tempa complexes of [Mn(L)] composition) the curve obtained by plotting $1/T_{1p}$ for the samples with [L]>[$Mn^{2+}$] as a function of $Mn^{2+}$ concentration gives a straight line, with a slope that is equal to the relaxivity of the complex, whereas the inflection point on the curve can be used to calculate the concentration of the ligand stock solution by using the standardized $Mn^{2+}$ stock solution concentration (or the other way around to crosscheck the concentration of the $Mn^{2+}$ stock solution by using that of the standardized ligand stock).

**$^1$H NMRD and $^{17}$O NMR Measurements.** The proton $1/T_1$ $^1$H NMRD profiles were measured on a fast field-cycling Stelar SmartTracer relaxometer (Mede, Pv, Italy) over a continuum of magnetic field strengths from 0.00024 to 0.25 T (corresponding to 0.01−10 MHz proton Larmor frequencies). The relaxometer operates under computer control with an absolute uncertainty in $1/T_1$ of ±1%. The temperature was controlled with a Stelar VTC-91 airflow heater equipped with a calibrated copper−constantan thermocouple (uncertainty of ±0.1 K). Additional data points in the range of 15−70 MHz were obtained on a Stelar Relaxometer equipped with a Bruker WP80 NMR electromagnet adapted to variable-field measurements (15−80 MHz proton Larmor frequency). For these $^1$H data, a 7.1 mM solution of the [Mn(nompa)]$^+$ complex in nondeuterated water was utilized. The exact complex concentration was determined by the BMS shift method at 11.7 T.[28] $^{17}$O NMR measurements were recorded on a Bruker Avance III spectrometer (11.7 T) equipped with a 5 mm probe and standard temperature control unit. A 15.0 mM aqueous solution of [Mn(nompa)]$^+$ containing 2.0% of the $^{17}$O isotope (Cambridge Isotope) was used. The observed transverse relaxation rates were calculated from the signal width at half-height.

**X-ray Crystallography.** The $Mn^{2+}$ complex formed with the tacn derivative was obtained by mixing a solution of 50 mg of nompa·2HCl ($C_{13}H_{20}N_4O_2 \cdot 2.1$ HCl·0.8 $H_2O$; 0.156 mmol) in 15 mL of $H_2O$ with 1 equiv of $Mn^{2+}$ perchlorate hexahydrate (0.156 mmol). The pH was adjusted to 6.5 by addition of NaOH (1 M solution), and the mixture was refluxed for 2 days (pH of the solution was kept at 6.5 throughout the reaction). The single crystals of the $Mn^{2+}$ complex used for the X-ray investigation were obtained by slow evaporation of this aqueous solution. Single-crystal X-ray diffraction data of $[Mn_2(nompa)_2(H_2O)_2](ClO_4)_2$ were collected by François Michaud at 300 K on an X-CALIBUR-2 CCD 4-circle diffractometer (Oxford Diffraction) with graphite-monochromatized Mo K$\alpha$ radiation ($\lambda$ = 0.71073). Unit-cell determination and data reduction, including interframe scaling, Lorentz, polarization, empirical absorption, and detector sensitivity corrections, were carried out using attached programs of Crysalis software (Oxford Diffraction).[29] Structures were solved by direct methods and refined by the full-matrix least-squares method on $F^2$ with the SHELXL[30] suite of programs. A non-coordinated perchlorate anion and the macrocyclic unit containing N1, N2, and N3 show positional disorder with two positions having equal


dx.doi.org/10.1021/ic500231z | Inorg. Chem. 2014, 53, 5136−5149

**Scheme 1. Synthesis of the Three Studied Ligands**[a]

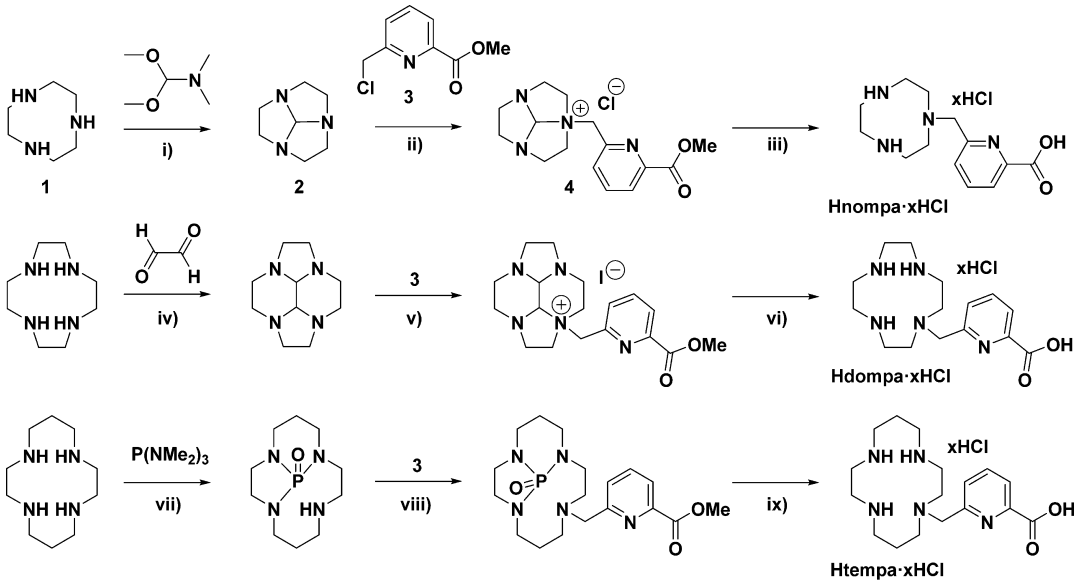


[a](i) toluene, RT, 12 h; (ii) THF, RT, 8 d; (iii) MeOH/HCl 12 M (1:1); HCl 3 M solution reflux; (iv) MeOH, 0°C to RT; (v) NaI, THF, 5 d; (vi) $NH_2NH_2$, $H_2O$ reflux 4h; ccHCl solution reflux, 24 h; ion exchange resin; (vii) $P(NMe_2)_3$; $CCl_4$; NaOH; (viii) $CH_3CN$; $K_2CO_3$; (ix) HCl 6M, reflux 12 h, ion exchange resin.

occupancy factors. The hydrogen atoms were identified at the last step and refined under geometrical restraints and isotropic U-constraints.[31] CCDC 982110 contains the supplementary crystallographic data for this paper. These data can be obtained free of charge from the Cambridge Crystallographic Data Centre via www.ccdc.cam.ac.uk/data_request/cif. Crystal data and structure refinement details: Formula: $C_{26}H_{42}Cl_2Mn_2N_8O_{14}$; MW: 871.46; crystal system: monoclinic; space group: $P2_1/n$; $a$ = 13.7909(6) Å; $b$ = 15.8672(8) Å; $c$ = 16.9957(7) Å; $\beta$ = 104.242(4)°; $V$ = 3604.7(3) Å$^3$; $F(000)$ = 1800; $Z$ = 4; $D_{calc}$ = 1.606 g cm$^{-3}$; $\mu$ = 0.925 mm$^{-1}$; $\theta$ range = 2.8443−31.5921°; $R_{int}$ = 0.0567; reflections measured: 27382; reflections observed: 3943; GOF on $F^2$ = 0.868; $R_1$ = 0.0461; $wR_2$ (all data) = 0.1105; largest differences peak and hole: 0.411 and −0.274 eÅ$^{-3}$.

**Computational Methods.** All calculations presented in this work were performed employing the Gaussian 09 package (revision B.01).[32] Full geometry optimizations of the $[Mn(nompa)(H_2O)]\cdot xH_2O$ ($x$ = 0 or 2) were performed in aqueous solution employing DFT within the hybrid meta-GGA approximation with the TPSSh exchange-correlation functional.[33] For geometry optimization purposes, we used the standard Ahlrichs' valence double-$\xi$ basis set including polarization functions (SVP).[34] No symmetry constraints have been imposed during the optimizations. The highest spin state was considered as the ground state (sextuplet, $3d^5$). Spin contamination[35] was assessed by a comparison of the expected difference between $S(S+1)$ for the assigned spin state ($S(S+1)$ = 8.75 for the mononuclear $Mn^{2+}$ complexes investigated here) and the actual value of $\langle S^2\rangle$.[36] The results obtained indicate that spin contamination is negligible for systems investigated in this work [$\langle S^2\rangle$-S(S+1)<0.0050]. The stationary points found on the potential energy surfaces as a result of geometry optimizations were tested to represent energy minima rather than saddle points via frequency analysis.

Isotropic $^{17}O$ and $^{1}H$ HFCCs in the $[Mn(nompa)(H_2O)]\cdot 2H_2O$ system were calculated in aqueous solution with unrestricted DFT methods by employing the TPSSh exchange−correlation functional. For the description of C, H, N, and O, we used the EPR-III basis sets of Barone,[37] which is a triple-$\zeta$ basis set including diffuse functions, double d-polarizations, and a single set of f-polarization functions, together with an improved s-part to better describe the nuclear region. For Mn, we used the aug-cc-pVTZ-J basis set developed by Sauer for the calculation of EPR HFCCs, which is described by a (25s17p10d3f2g)/[17s10p7d3f2g] contraction scheme, and contains four tight s-, one tight p-, and one tight d-type functions.[38] To avoid problems with the convergence of the SCF procedure we used a quadratically convergent SCF procedure when first order SCF did not achieve convergence (by using the scf = xqc keyword in g09). The default values for the integration grid (75 radial shells and 302 angular points) and the SCF energy convergence criteria ($10^{-8}$) were used in all calculations.

Throughout this work, solvent effects were included by using the polarizable continuum model (PCM), in which the solute cavity is built as an envelope of spheres centered on atoms or atomic groups with appropriate radii. In particular, we used the integral equation formalism (IEFPCM) variant as implemented in Gaussian 09.[39]

## RESULTS AND DISCUSSION

**Ligand Syntheses.** The control of the *N*-selective substitution of polyazacycloalkanes remains a current challenge in ligand synthesis despite the huge progress of the subject due to the contributions of different research groups. Among the various methods giving access to mono-*N*-functionalized tacn,[40] cyclen, and cyclam[41] derivatives, we have chosen a general approach involving the protection−functionalization−deprotection sequence. Due to the inherent properties of each azamacrocycle, the protection step has been adapted to each chelator synthesis. The synthesis of Hnompa, which is reported here for the first time, is shown in Scheme 1. Reaction of tacn with *N*-dimethoxymethyl-*N*,*N*-dimethylamine gave rise to the formation of the already known orthoamide 1,4,7-triazatricyclo-[5.2.1.0$^{4,10}$]decane **2**, which is an effective intermediate in the monoalkylation of tacn with halogenoalkane derivatives.[42] The subsequent alkylation step proceeded by stoichiometric addition of 6-chloromethylpyridine-2-carboxylic acid methyl ester[25] to a THF solution of the previous protected triazamacrocycle. The resulting monoammonium salt **4** was easily isolated after precipitation in the THF reaction medium. The deprotection step under acidic conditions and concomitant hydrolysis of the ester function led to the final 6-((1,4,7-triazacyclonan-1-yl)methyl)picolinic acid ligand as its hydrochloride form. Ligand Hdompa (6-((1,4,7,10-tetraazacyclo-


dx.doi.org/10.1021/ic500231z | Inorg. Chem. 2014, 53, 5136−5149

**Table 1. Protonation and Stability Constants and pMn Values (Calculated at pH = 7.4, $c_L$ = 10 μM, and $c_{Mn2+}$ = 1 μM) Characterizing the Equilibrium Involving the nompa$^-$, dompa$^-$, and tempa$^-$ Ligands and Their $Mn^{2+}$ and $Cu^{2+}$ Complexes ($I$ = 0.15 M NaCl, $T$ = 25 °C)**

| | nompa$^-$ | tacn[a] | dompa$^-$ | cyclen | tempa$^-$ | cyclam[e] |
|---|---|---|---|---|---|---|
| log $K_1^H$ | 11.33(3) | 10.50 | 11.22(2); 10.46[c] | 11.05(2) | 12.13(1); 11.55[c] | 11.29 |
| log $K_2^H$ | 7.30(5) | 6.80 | 9.38(5); 9.26[c] | 9.78(3) | 10.20(1); 10.11[c] | 10.19 |
| log $K_3^H$ | 2.49(5) | | 3.39(6) 3.23[c] | | 2.86(2); 2.71[c] | 1.61 |
| log $K_4^H$ | | | | | 1.30(2); 1.70[c] | 1.91 |
| Σ log $K_2^H$ | 18.63 | 17.30 | 20.60; 19.72[c] | 20.83 | 22.33; 21.66[c] | 21.48 |
| log $K_{MnL}$ | 10.28(1) | 8.33 | 14.48 (1) | 8.76(1) | 12.53(1) | see *f* below |
| log $K_{MnL}^H$ | | | 4.03(6) | | 5.69(8) | |
| log $K_{MnL}^{OH}$ | 11.94(2) | | | | | |
| pMn | 7.08 | 6.37 | 9.07 | 6.00 | 6.29 | |
| log $K_{CuL}$ | 21.07(1) | 17.40[b] | 25.06(1); 24.0[c] | 23.4[d] | 25.5[c] | 28.09 |
| log $K_{CuL}^H$ | | | 1.86(2); 1.83[c] | | 2.17[c] | |
| log $K_{CuL}^{OH}$ | 11.90(1) | | 9.85[c] | | 11.15[c] | |

[a] $I$ = 0.10 M $KNO_3$, $T$ = 20 °C, ref 46. [b] $[Cu(L)_2]$ and $[Cu(L)_2(OH)_2]$ complexes were also found in solution, $I$ = 0.50 M $KNO_3$, ref 47. [c] $I$ = 0.1 M $KNO_3$, ref 23. [d] $I$ = 0.10 M $NaNO_3$, ref 48. [e] $I$ = 0.10 M KCl, ref 49. [f] The stability constant could not be determined because of the precipitation process that occurred parallel with the complexation at high pH.

dodecan-1-yl)methyl)picolinic acid) was synthesized using the bisaminal tool,[43] an approach widely exploited in previous works.[44] Concerning the cyclam derivative, as previously described, the triprotection via the phosphoramide tripode allowed the selective introduction of the picolinate group on the macrocycle to yield 6-((1,4,8,11-tetraazacyclotetradecan-1-yl)methyl)picolinic acid (Htempa) after treatment.[45]

**Equilibrium Studies: Stability Constants of $Mn^{2+}$ and $Cu^{2+}$ Complexes.** The protonation constants of the ligands as well as the stabilities of the $Mn^{2+}$ complexes were assessed by direct pH-potentiometric titration at 25 °C, using ionic strength adjusted to 0.15 M NaCl. The protonation constants of the ligands are listed and compared to those of the parent tacn, cyclen, and cyclam macrocyclic polyamines in Table 1. The data collected in Table 1 agree well with the data published previously for the dompa$^-$ and tempa$^-$ ligands except for the first protonation constant, which was found to be somewhat higher (0.6–0.7 log $K$ units) than the ones determined in 0.1 M $KNO_3$. This small difference is very likely to be attributed to the different titration protocols (calibration routine, determination of the Irving correction factor, and slightly different p$K_w$ value that was determined in the titration cell following the calibration ahead of the ligand titration). The data shown in Table 1 indicate that the substitution of the picolinate pendant arm does not significantly affect the basicity of the nitrogen donor atoms (Σ log $K_2^H$) of the ligands. As stated earlier,[23] the third protonation constant determined can be assigned to the picolinate moiety, and the fourth protonation process of the tempa$^-$ ligand occurs on the third nitrogen atom of the macrocycle. Due to the larger size of the macrocycle, the decreased charge repulsion between the protonated nitrogen atoms allows the protonation to occur at low pH (pH = 1.3), but this is not observed for dompa$^-$ and nompa$^-$. $^1$H NMR studies performed in the pH range of 1.9–1.4 evidence significant chemical shifts in the macrocycle proton signals, whereas the proton signals of the picolinate arm remain less affected (Figures S1 and S2, Supporting Information). This clearly confirms that the fourth protonation occurs on a nitrogen atom of the macrocycle.

The stability constants of the $Mn^{2+}$ complexes were assessed from the direct titration data (titration points were acquired after 1 min equilibration time) as the preliminary $T_1$ relaxation studies indicated fast complexation between the ligands and the $Mn^{2+}$ ion (the $T_1$ values measured approximately 1 min, 1 h, and 24 h after sample preparation in the pH range where the complexation occurs were found to be identical). In the case of the $Mn^{2+}$:nompa system, the equilibrium can be described by taking into account the formation of $[Mn(nompa)]^+$ and $[Mn(nompa)(OH)]$ complexes, whereas for the dompa and tempa systems the monoprotonated complex ($[MnH(L)]^{2+}$) was also detected. In a good agreement with the absence of the water molecule bound in the inner coordination sphere of the $Mn^{2+}$ complexes of dompa and tempa, the formation of ternary hydroxo complexes was not detected. The species distribution diagrams shown in Figure 1 indicate that the complexation

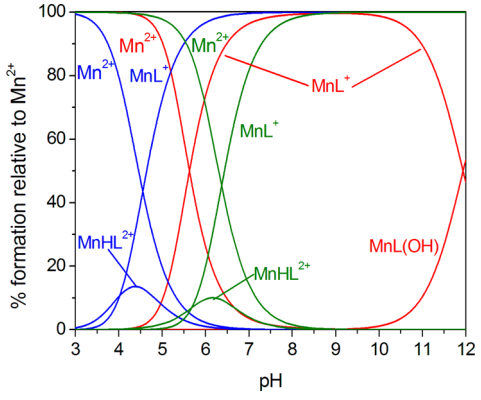


**Figure 1.** Speciation distribution curves of $Mn^{2+}$ complexes in the presence of nompa (red), dompa (blue), and tempa (green) ligands ($[Mn^{2+}]_{tot}$ = $[L]_{tot}$ = 0.0025 mM).

involving the dompa$^-$ ligand occurs above pH ~ 3.0. However, for nompa$^-$, complexation starts at pH > 4.0, and the $[Mn(tempa)]^+$ complex starts to form only around pH = 5.0. As shown in the data presented in Table 1, the attachment of a picolinate moiety to the macrocyclic polyamine backbone resulted in a noticeable increase in the stability of their $Mn^{2+}$ complexes. A moderate increase in the stability of $[Mn(L)]^+$ complexes was detected for the nompa$^-$ ligand, whereas for dompa, the increase is more pronounced as the stability constant increased by almost 6 log $K$ units. The stability of the


dx.doi.org/10.1021/ic500231z | Inorg. Chem. 2014, 53, 5136–5149

$[Mn(cyclam)]^{2+}$ complex is not available in the literature and could not be determined in the current study due to the formation of a precipitate during the titration.

This increase is also visible if one compares the pMn values ($pMn = -\log[Mn]_{free}$) of the complexes calculated at pH = 7.4 using 10 $\mu$M ligand and 1 $\mu$M $Mn^{2+}$ ion concentrations and the protonation constants of the ligands and stability constants of the complexes, as suggested originally by Raymond and co-workers for $Gd^{3+}$ complexes.[50] The pMn values of the $Mn^{2+}$ complexes formed with tacn and cyclen polyamines are nearly equal to 6, which indicates that complexation is more or less absent in solution under the conditions listed above. However, the pMn values of the monopicolinate derivatives are higher than those of the parent polyamines, which can be easily outlined by calculating the difference $\Delta pM_n$ = [pMn(tempa) − pMn(cyclam)] = 0.29 for the tempa (if one assumes no complexation between the $Mn^{2+}$ ion and the cyclam ligand, pMn = 6.00), ΔpMn = pMn(nompa) − pMn(tacn) = 0.71 and ΔpMn = pMn(dompa) − pMn(cyclen) = 3.07. The difference found for the $[Mn(dompa)]^+$ complex is somewhat greater than 3 pMn units, which indicates that the 12-membered macrocyclic tetraamine unit is the most suitable for the $Mn^{2+}$ ion as far as the stability constants of the complexes are concerned.

Because the $Cu^{2+}$ ion was used as a scavenger metal ion in the kinetic experiments, the stability constant of the $[Cu(nompa)]^+$ complex was also determined in the current study. In order to crosscheck the stability constant computed by using a competition method involving the edta ligand published earlier,[23] the stability constant of $[Cu(dompa)]^+$ was also redetermined. The $[Cu(nompa)]^+$ and $[Cu(dompa)]^+$ complexes were titrated by using pH-potentiometry at first. In the $Cu^{2+}$:nompa system at pH < 11.0, only the $[Cu(nompa)]^+$ complex was detected, which had already formed quantitatively at acidic pH (below pH < 1.8). In strongly basic solutions, the $[Cu(nompa)]^+$ complex was found to form a mixed hydroxo complex with [Cu(nompa)(OH)] composition. On the basis of these results, out-of-cell samples were prepared and equilibrated in strongly acidic media for a week ($H^+$ concentration was in the range of 7.43−157 mM). Subsequently, the visible absorption spectra were acquired in the wavelength range of 350−850 nm ($\lambda_{max}$ = 670 nm) (Figure 2). A total of 21 wavelengths were selected near the $\lambda_{max}$, and the molar absorption coefficients of the $Cu^{2+}$ and $[Cu(nompa)]^+$ species were used to determine the stability constant (Table 1, fitting parameter = 0.0083 Abs for the 168 data points fitted). A similar procedure (six samples in the acid concentration range of 0.1052 to 1.010 M by fitting 128 data points from 27 selected wavelengths near the $\lambda_{max}$ = 620 nm) was applied for the $[Cu(dompa)]^+$ system, but in this case, the monoprotonated $[CuH(dompa)]^{2+}$ species was found to form in strongly acidic medium (fitting parameter = 0.0075 Abs for the 128 data points fitted, see Figure S4, Supporting Information). The deprotonation of $[CuH(dompa)]^{2+}$ to form $[Cu(dompa)]^+$ was followed by pH-potentiometry (Figure S6, Supporting Information) and the constant characterizing the equilibrium $[Cu(dompa)]^+ + H^+ = [CuH(dompa)]^{2+}$ determined (Table 1). The protonation constants of $[Cu(dompa)]^{2+}$ determined in the present and previous studies are in excellent agreement, taking into account the slightly higher overall basicity of the dompa ligand found in the current study ($\Delta \Sigma \log K_3^H = 1.04$); the difference observed in the $[Cu(dompa)]^{2+}$ complex stability ($\Delta \log K = 1.06$) is also acceptable. These results confirm that $Cu^{2+}$ ion forms a more stable complex with the 12-membered monopicolinate derivative, similarly to that found for the $Mn^{2+}$ complex. However, the 14-membered $tempa^-$ ligand forms an even more stable complex with the $Cu^{2+}$ ion,[23] and the cyclam 14-membered macrocyclic ring seems to be not the optimal one for $Mn^{2+}$ encapsulation.

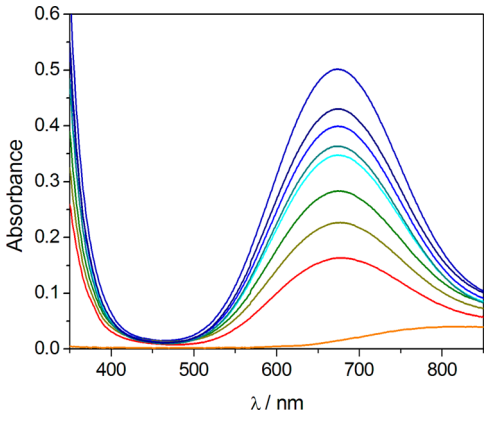


**Figure 2.** Absorption spectra of the $Cu^{2+}$−nompa system as a function of $[H^+]$ ($CuCl_2$ solution only, $[H^+]$ = 0.1572, 0.1324, 0.1076, 0.08287, 0.06709, 0.05696, 0.04795, and 0.007430 M upward; $[Cu^{2+}]$ = 0.002868 M and [nompa] = 0.002985 M, $T$ = 25 °C).

**Kinetic Inertness of the $[Mn(nompa)]^+$ and $[Mn(dompa)]^+$ Complexes.** The kinetic inertness of the complexes considered for in vivo application is one of the most important factors to be studied, as all possible products of the dissociation are toxic at the concentration suitable for MRI investigation. The dissociation kinetics of the $Mn^{2+}$ complexes is typically studied by following the exchange reaction taking place between the complex and the $Zn^{2+}$-ion (at various concentrations and pH) followed by relaxometry. However, the metal exchange reactions of $[Mn(dompa)]^+$ and $[Mn(nompa)]^+$ complexes were found to occur within a few seconds in the studied pH range (pH = 3.67−4.65 for the dompa and 3.47−5.08 for the nompa complex). Thus, a stopped-flow method was utilized to study the dissociation reactions by using high excess of $Cu^{2+}$ (10−40 fold) as a scavenger to ensure the pseudo-first-order conditions. Scheme 2 indicates the possible pathways of dissociation through which the decomplexation of the $Mn^{2+}$ chelates may take place: spontaneous dissociation (1) characterized by the rate constant $k_0$; proton-assisted decomplexation (2a and 2b) characterized by the protonation constant $K_1^H$ (and rarely $K_2^H$) and rate constants $k_H$ and $k_H^H$; metal-ion-catalyzed dissociation (3a and 3b) characterized by the stability of dinuclear complexes $K_M$ and rate constant $k_M$ (the dissociation of the dinuclear intermediate may also proceed via the acid-catalyzed pathway described by $K_M^H$ and rate constant $k_M^H$).

When the exchanging metal ion is taken in a large excess the reaction rate can be expressed as follows:

$$-\frac{d[Mn(L)]_t}{dt} = k_{obs}[Mn(L)]_{tot} \quad (1)$$

where $k_{obs}$ is a pseudo-first-order rate constant, and $[Mn(L)]_{tot}$ is the total $[Mn(L)]^+$ concentration. The rate constants $k_{obs}$ are directly proportional to $[H^+]$ giving a straight line with positive intercept (Figure 3), but they were found to be independent of the $Cu^{2+}$ ion concentration (Figures S7 and S8, Supporting Information). This is not very surprising, because the denticity


dx.doi.org/10.1021/ic500231z | Inorg. Chem. 2014, 53, 5136−5149

**Scheme 2. Possible Reaction Mechanisms for the Decomplexation of the $Mn^{2+}$ Complexes[a]**

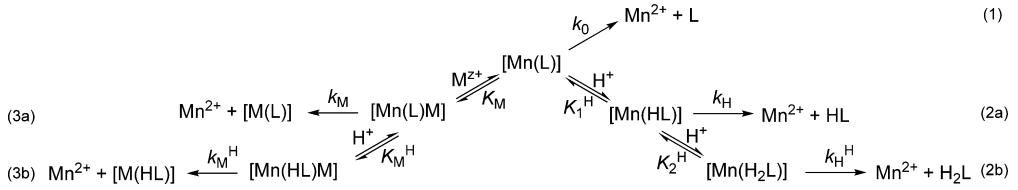


[a](where $K_1^H$ = [Mn(HL)]/[Mn(L)][$H^+$], $K_2^H$ = [Mn($H_2$L)]/[Mn(HL)][$H^+$], $K_M$ = [Mn(L)M]/[Mn(L)][M], and $K_M^H$ = [Mn(HL)M]/[Mn(L)M][$H^+$], whereas for the rate constants $k_1 = k_H \cdot K_1^H$, $k_2 = k_H^H \cdot K_1^H \cdot K_2^H$, $k_3 = k_M \cdot K_M$, and $k_4 = k_M^H \cdot K_M \cdot K_M^H$).

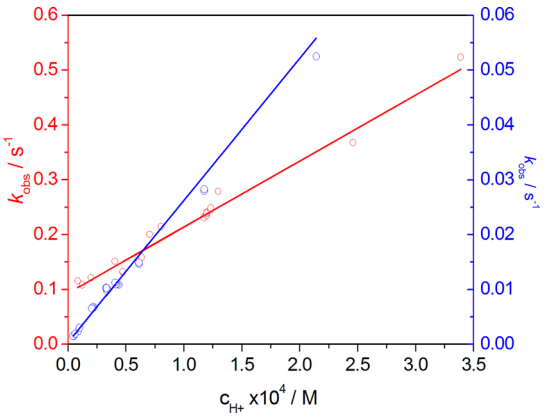


**Figure 3.** Dependence of the observed dissociation rate constants ($k_{obs}$) for [Mn(nompa)]$^+$ (red) and [Mn(dompa)]$^+$ (blue) on proton concentration. The line corresponds to the best fits with the parameters shown in Table 2. The dependence on $Cu^{2+}$ ion concentration was checked at several pH values and is included in the plot.

of the ligands studied are either lower (nompa$^-$) or equal (dompa$^-$) to the coordination number of the metal ion in the complexes (see below). The formation of the dinuclear key intermediate [Mn(L)Cu] requires a free donor atom in the complex capable of binding the exchanging metal ion, which is not the case for [Mn(nompa)]$^+$ and [Mn(dompa)]$^+$. Therefore, only the spontaneous- and proton-assisted dissociation pathways are operative for the $Mn^{2+}$ complexes of these monopicolinate ligands. From these considerations, the rates of the exchange reactions can be expressed by the following equation:

$$-\frac{d[Mn(L)]_t}{dt} = k_0[Mn(L)] + k_H[Mn(HL)] \quad (2)$$

Because the total concentration of complexed $Mn^{2+}$, $[Mn(L)]_t$, can be given as [Mn(L)] + [Mn(HL)], and taking account the expression for the protonation constant of the complex $K_1^H$, eqs 1 and 2 allow expressing the pseudo-first-order rate constant ($k_{obs}$) as in eq 3,

$$k_{obs} = k_0[Mn(L)] + k_H[Mn(HL)] = \frac{k_0 + k_1[H^+]}{1 + K_1^H[H^+]} \quad (3)$$

where $k_H \cdot K_1^H = k_1$. The two $Mn^{2+}$ complexes behave differently as far as the protonation equilibrium of the [Mn(L)] complexes are concerned, because [Mn(nompa)]$^+$ was not found to form a protonated complex, and existence of the protonated [Mn(Hdompa)]$^+$ species was confirmed by the equilibrium measurements described above. Nevertheless, the protonation constant ($K_1^H$) could not be determined from the kinetic data for any of the systems studied, and hence the term $K_1^H$ [$H^+$] in the denominator of eq 3 can be neglected. This allows us to simplify the latter equation to $k_{obs} = k_0 + k_1[H^+]$, which was used to evaluate the rate constants $k_0$ and $k_1$. Because the dissociation kinetics of [Mn(dompa)]$^+$ could be studied only in the pH range where the kinetically more labile monoprotonated complex exists in solution, for this system, the $k_0$ and $k_1$ rate constants correspond to the spontaneous and acid catalyzed dissociation of the protonated complex, respectively. The rate constants obtained by fitting the pseudo-first-order rate constant obtained at different $H^+$ concentrations and exchanging metal ion concentrations are compared to those published for [Mn(cdta)]$^{2-}$, [Mn(nota)]$^-$, [Mn(dota)]$^{2-}$, and some other $Mn^{2+}$-based CA candidates studied recently in Table 2.

The rates of acid catalyzed dissociation of the [Mn(nompa)]$^+$ and [Mn(Hdompa)]$^{2+}$ complexes are similar to those of other $Mn^{2+}$ complexes studied recently (e.g the $k_1$ of [Mn(nompa)]$^+$ is similar to that of [Mn(pcma)]$^+$, although the

**Table 2. Equilibrium Constants, Rate Constants, and Half-Lives of the Reactions Characterizing the Dissociation of $Mn^{2+}$ Complexes (25 °C, $I$ = 0.15 M NaCl, dmp buffer)**

| | $k_0$ ($s^{-1}$) | $k_1$ ($M^{-1}$ $s^{-1}$) | $k_2$ ($M^{-2}s^{-1}$) | $k_3$ ($M^{-1}$ $s^{-1}$) | $k_4$ ($M^{-2}s^{-1}$) | log $K_1^H$ | $K_M$[e] | $t_{1/2}$[f] (h) |
|---|---|---|---|---|---|---|---|---|
| nompa | 9.4(4) × $10^{-1}$ | 1203(58) | | | | | | 2.15 × $10^{-3}$ |
| dompa | 1.2(2) × $10^{-3}$ | 235(3) | | | | 4.02 | | 0.160 |
| cdta[a] | | 4.0 × $10^2$ | | | | | | |
| | | (3.2 × $10^2$) | | | | | | |
| | | | | | 79 | 12 (15) | | |
| pcma[b] | | 2020 | 8.0 × $10^7$ | | | 4.95 | | 2.4 |
| 15-Py-aneN$_5$[c] | | 423 | 1.0 × $10^7$ | | 1.7 × $10^4$ | 4.27 | | 11.4 |
| nota[d] | 2.6 × $10^{-6}$ | 0.78 | | 1.1 × $10^{-5}$ | | 2.87 | 3.6 | 74 |
| dota[d] | 1.8 × $10^{-7}$ | 4.0 × $10^{-2}$ | 1.6 × $10^3$ | 1.5 × $10^{-5}$ | | 4.26 | 68 | 1037 |

[a]Taken from ref 51. [b]ref 17. [c]ref 12. [d]ref 52. [e]M = $Cu^{2+}$ or $Zn^{2+}$; [f]pH = 7.4; the concentration of the exchanging metal ion used in the calculations was 1 × $10^{-5}$ M ($Cu^{2+}$ ion for cdta and $Zn^{2+}$ for all other complexes).


dx.doi.org/10.1021/ic500231z | Inorg. Chem. 2014, 53, 5136−5149

$k_1$ of the nonaquated $[Mn(Hdompa)]^{2+}$ complex is similar to those of $[Mn(cdta)]^{2-}$ and $[Mn(15aneN_5)]^{2+}$ complexes. However, these $Mn^{2+}$ complexes of the monopicolinate ligands cannot be regarded for in vivo applications because of their unsatisfactory kinetic inertness, which is a consequence of the pronounced spontaneous dissociation. The data in Table 2 indicate that the spontaneous dissociation of the $[Mn(nompa)]^{+}$ and $[Mn(Hdompa)]^{2+}$ complexes is not negligible, while it is either not detected ($[Mn(pcma)]^{+}$, $[Mn(cdta)]^{2-}$ and $[Mn(15aneN_5)]^{2+}$) or has an insignificant contribution to the overall dissociation reaction (e.g., [Mn(nota)]- or [Mn(dota)]2-) for non-picolinate derivatives. As a result of the high rate constants of spontaneous dissociation, the half-lives of the dissociation calculated at pH = 7.4 for the $Mn^{2+}$ complexes of the monopicolinates are at least 2 orders of magnitude lower than the those of the complexes listed in Table 2.

The pronounced spontaneous dissociation rate of decomplexation of $[Mn(nompa)]^{+}$ complex was found to depend on the quality of the buffer used in the study. The dmp and nmp buffers are frequently selected for kinetic studies because the second protonation of these buffers occurs in the pH range where the dissociation of the complexes are often studied ($\log K^2_H$ = 4.19 (0.01) for dmp and $\log K^2_H$ = 4.92 (0.02) in 0.15 M NaCl for nmp), and they are also known to behave as noncoordinating buffers (especially when the dissociation of lanthanide (III) complexes are studied). Furthermore, the use of a mixture of dmp and nmp allows a relatively wide and useful pH range (3.2−5.9) to be covered. The nature of the buffer (or its concentration) usually has no effect on the rate of dissociation, but clearly this is not the case for the $[Mn(nompa)]^{+}$ complex, as the rates of the dissociation reactions were found to strongly depend on the nature and the concentration of the nmp buffer. However, the rates remained unaffected by the concentration of dmp (Figures S9 and S10, Supporting Information). This can be explained by the formation of a ternary complex between $[Mn(nompa)]^{+}$ and presumably the monoprotonated form of nmp, as the diprotonated buffer cannot interact with the complex, and the unprotonated nmp cannot act as a "proton-transfer" agent. Most likely, the Hnmp form of the buffer is involved in an effective proton transfer to one of the donor atoms of the nompa ligand in its $Mn^{2+}$ complex. Our attempts to characterize the reaction intermediate by means of relaxometry at pH = 7.1 failed, as the relaxivity of the $[Mn(nompa)]^{+}$ complex in the presence and in the absence of 50 mM Hnmp buffer turned out to be identical. Nevertheless, the effect of the nmp buffer on the dissociation rates suggest that the protonation of the $[Mn(nompa)]^{+}$ complex is facilitated by a proton transfer occurring in a $[Mn(nompa)(Hnmp)]^{2+}$ ternary complex, which in turn results in the increase of the rate of dissociation. These results indicate that dissociation kinetics studies of $Mn^{2+}$ complexes with the commonly used nmp buffer might return kinetic data based on which the kinetic inertness of the complexes can be misjudged, as the given buffer may accelerate the rates of dissociation. This effect is more likely to occur in the case of positively charged complexes being coordinatively unsaturated, so that ternary complex formation is favored.

**X-ray Crystal Structure of $[Mn_2(nompa)_2(H_2O)_2](ClO_4)_2$.** Single crystals of the $Mn^{2+}$ complex of $nompa^{-}$ were obtained by slow evaporation of an aqueous solution of the complex at neutral pH (prepared in situ by mixing stoichiometric amounts of the ligand and $Mn^{2+}$ perchlorate). Crystals contain the $[Mn_2(nompa)_2(H_2O)_2]^{2+}$ cation and two uncoordinated perchlorate anions. Figure 4 shows a view of the complex cation, whereas bond distances of the metal coordination environments are given in Table 3. Each of the $Mn^{2+}$ ions is directly coordinated to the six donor atoms of a $nompa^{-}$ ligand and an oxygen atom of a neighboring $nompa^{-}$ ligand that is bridging the two $Mn^{2+}$ centers. Coordination number seven is completed by the oxygen atom of a coordinated water molecule. The binuclear $[Mn_2(nompa)_2(H_2O)_2]^{2+}$ entity is stabilized by the presence of bridging bidentate carboxylate groups ($\mu$−$\eta^1$-carboxylate).[53] Additionally, each of the uncoordinated oxygen atoms of picolinate groups (O2 and O4) is involved in an intramolecular hydrogen-bonding interaction with a coordinated water molecule [O6···O2 2.880(5) Å, O6−H6W···O2 2.08(3) Å, O6−H6W···O2 158(6)°; O5···O4 2.831(4) Å, O5−H5W···O4 2.02(3) Å, O5−H5W···O4 161(5)°] and a NH group of the macrocycle [N3A···O4 3.025(4) Å, N3A-H3M···O4 2.27 Å, O3A-H3M···O4 140.4°; N7···O2 3.055(4) Å, N7−H7···O2 2.31 Å, N7−H7···O2 138.9°]. The distance between the two $Mn^{2+}$ ions in $[Mn_2(nompa)_2(H_2O)_2]^{2+}$ amounts to 3.76 Å. The three five-membered chelate rings formed upon coordination of the tacn moiety adopt identical configurations, two ($\delta\delta\delta$) and ($\lambda\lambda\lambda$) enantiomers being present in the crystal lattice.[54]

For each $Mn^{2+}$ ion, one of the distances to a nitrogen donor atom of the macrocycle [Mn1−N1A and Mn2−N5] is clearly longer than the remaining bond distances of the metal coordination environments, which points to a rather weak interaction between the metal ion and these donor atoms. The distances between the metal ions and the remaining two

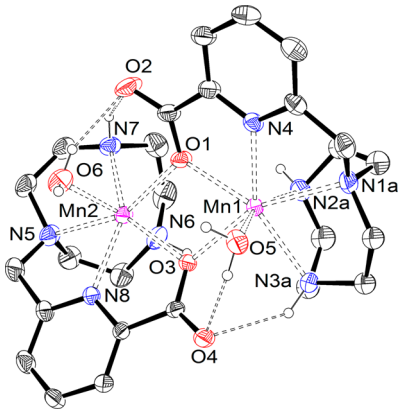


**Figure 4.** View of the structure of the $[Mn_2(nompa)_2(H_2O)_2]^{2+}$ cation present in crystals of $[Mn_2(nompa)_2(H_2O)_2](ClO_4)_2$. The ORTEP plot is at the 30% probability level. Hydrogen atoms attached to carbon atoms are omitted for simplicity.

**Table 3. Bond Distances (Å) of the Metal Coordination Environments in $[Mn_2(nompa)_2(H_2O)_2]^{2+a}$**

| | | | |
|---|---|---|---|
| Mn1−N1A | 2.446(3) | Mn2−N5 | 2.466(3) |
| Mn1−N2A | 2.276(3) | Mn2−N6 | 2.280(3) |
| Mn1−N3A | 2.307(3) | Mn2−N7 | 2.299(3) |
| Mn1−N4 | 2.247(3) | Mn2−N8 | 2.259(3) |
| Mn1−O1 | 2.309(2) | Mn2−O1 | 2.273(2) |
| Mn1−O3 | 2.261(2) | Mn2−O3 | 2.324(2) |
| Mn1−O5 | 2.276(3) | Mn2−O6 | 2.246(3) |

[a]Refer to Figure 4 for the labeling scheme.


dx.doi.org/10.1021/ic500231z | Inorg. Chem. 2014, 53, 5136−5149

nitrogen atoms of the macrocycle are close to those observed in binuclear $Mn^{2+}$ complexes containing tacn moieties[14,55] and longer than those typically observed for mononuclear six-coordinate $Mn^{2+}$-tacn derivatives.[56] The distances to the donor atoms of the picolinate moieties are also close to those observed in $Mn^{2+}$ complexes containing this binding motif.[57]

The most common coordination polyhedron for heptacoordinate transition-metal complexes is the pentagonal bipyramid, followed by the capped trigonal prism and the capped octahedron.[58] In $[Mn_2(nompa)_2(H_2O)_2]^{2+}$, the coordination polyhedra appear to be rather distorted, and an unequivocal assignment of a particular coordination polyhedron is not possible. This is confirmed by performing continuous shape measures with the assistance of the SHAPE program.[59,60] The analysis of the coordination polyhedra in $[Mn_2(nompa)_2(H_2O)_2]^{2+}$ provides very similar shape measures for the three coordination polyhedra: ca. 2.6 for a pentagonal bipyramid and a capped trigonal prism and ca. 2.7 for a capped octahedron. (The shape measure S(A) = 0 for a structure is fully coincident in shape with the reference polyhedron and the maximum allowed value of S(A) is 100.)

**Variable Temperature $^1$H NMRD and $^{17}$O NMR Measurements.** The efficiency of a paramagnetic complex as a CA is estimated by its proton relaxivity, $r_{1p}$, which refers to the relaxation enhancement of water protons promoted by a 1 mM concentration of the paramagnetic metal ion. The $r_{1p}$ values obtained for the $Mn^{2+}$ complexes of tempa$^-$, dompa$^-$, and nompa$^-$ at 20 MHz, 298 K, and pH = 8.08 are 1.33, 1.50, and 3.32 $mM^{-1}\cdot s^{-1}$, respectively (Figure S11, Supporting Information). The relaxivities of $[Mn(tempa)]^+$ and $[Mn(dompa)]^+$ are considerably lower than that of the complex with nompa$^-$, in line with the absence of coordinated water molecules. In the case of $[Mn(nompa)]^+$, its relaxivity is consistent with the presence of one water molecule in the $Mn^{2+}$ inner coordination sphere. Indeed, the relaxivity of $[Mn(nompa)(H_2O)]^+$ at 20 MHz and 298 K (3.32 $mM^{-1}\ s^{-1}$) is quite similar to that of $Mn^{2+}$ complexes containing an inner-sphere water molecule (i.e., $[Mn(edta)]^{2-}$).[18] These results indicate that this family of $Mn^{2+}$ complexes is six-coordinated, a water molecule completing the metal ion coordination environment in the complex with the pentadentate ligand nompa$^-$. This is in contrast to the X-ray crystal structure of the $[Mn(nompa)(H_2O)]^+$ complex, were the metal ion is seven-coordinated (see above). The relaxivity of $[Mn(nompa)(H_2O)]^+$ remains constant in the pH range of 7.1−9.9 and increases below pH 7 due to the dissociation of the complex and metal ion release (Figure S12, Supporting Information).

Nuclear magnetic relaxation dispersion ($^1$H NMRD) profiles of an aqueous solution of $[Mn(nompa)(H_2O)]^+$ (pH = 7.2) were measured at 298 and 310 K in the proton Larmor frequency range of 0.01−70 MHz, corresponding to magnetic field strengths varying between $2.343 \times 10^{-4}$ and 1.645 T (Figure 5). The relaxivity of $[Mn(nompa)(H_2O)]^+$ decreases with increasing temperature, a behavior typical of small chelates in which fast rotation of the complex in solution limits proton relaxivity (Figure 5). This is also confirmed by the temperature dependence of the relaxivity measured at 20 MHz in the temperature range of 280−321 K (Figure S13, Supporting Information). The $^1$H NMRD profiles show a single dispersion between 1 and 10 MHz, which points to a negligible scalar contribution to $^1$H relaxivity.[15b] The reduced transverse $^{17}$O NMR relaxation rates and chemical shifts measured for $[Mn(nompa)(H_2O)]^+$ are presented in Figure 6. The $1/T_{2r}$ values increase with decreasing temperature, which points to a relatively short residence time of the inner-sphere water molecule.

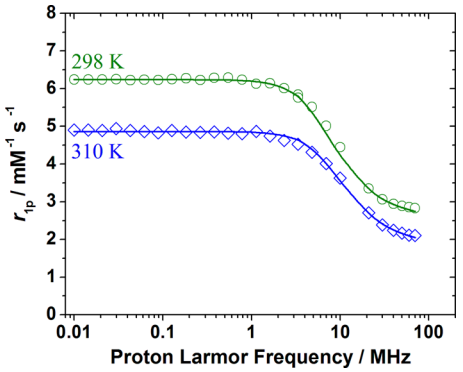


**Figure 5.** $^1$H NMRD profiles recorded at different temperatures for $[Mn(nompa)(H_2O)]^+$. The lines represent the fit of the data as explained in the text.

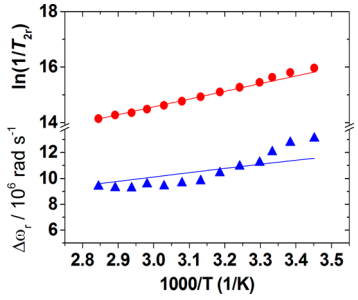


**Figure 6.** Reduced transverse (red ●) $^{17}$O NMR relaxation rates and $^{17}$O NMR chemical shifts (blue ▲) measured for $[Mn(nompa)(H_2O)]^+$ at 11.74 T. The lines represent the fit of the data as explained in the text.

A simultaneous fitting of the $^1$H NMRD and $^{17}$O NMR data of $[Mn(nompa)(H_2O)]^+$ was performed with the sets of equations given in the Supporting Information. Some parameters were fixed during the fitting procedure: the distance of closest approach for the outer-sphere contribution $a_{MnH}$ was fixed at 3.6 Å,[62] whereas the distance between the proton nuclei of the coordinated water molecule and the $Mn^{2+}$ ion ($r_{MnH}$) was fixed at 2.77 Å, which corresponds to the average Mn···H distance obtained from our DFT calculations described below (Table 4). The number of water molecules in the inner coordination sphere of $Mn^{2+}$ was fixed to $q = 1$. The parameters obtained from the fittings are listed in Table 4, and the curve fits are shown in Figures 5 and 6. The value obtained for the diffusion coefficient, $D^{298}_{MnH}$, is close to that for self-diffusion of water molecules in pure water ($2.3 \times 10^{-9}$ $m^2\cdot s^{-1}$),[63] indicating that they are dominated by the rapid diffusion of water molecules. The rotational correlation time ($\tau_R^{298}$) obtained from the analysis of the $^1$H NMRD profiles is very similar to those reported for small $Mn^{2+}$ complexes, but clearly smaller than that reported for the binuclear $[Mn_2(enota)(H_2O)_2]$ complex. The values of the parameters characterizing the electron spin relaxation, the electronic correlation time for the modulation of the zero-field-splitting interaction ($\tau_V$), its activation energy ($E_V$), and the mean square zero-field-splitting energy ($\Delta^2$) also take reasonable values.


dx.doi.org/10.1021/ic500231z | Inorg. Chem. 2014, 53, 5136−5149

**Table 4. Parameters Obtained from the Simultaneous Analysis of $^{17}O$ NMR and $^{1}H$ NMRD Data**

| | nompa$^-$ | enota[b] | meno2a[c] |
|---|---|---|---|
| $k_{ex}^{298}$ ($10^6$ s$^{-1}$) | 2768 ± 371 | 55.0 | 626 |
| $\Delta H^{\ddagger}$ (kJ mol$^{-1}$) | 20.5 ± 3.8 | 20.5 | 11 |
| $\tau_R^{298}$ (ps) | 51.2 ± 1.5 | 85 | 36 |
| $E_r$ (kJ mol$^{-1}$) | 21.3 ± 19 | 18 | 22.8 |
| $\tau_v^{298}$ (ps) | 32.8 ± 19.0 | 7.7 | 21.4 |
| $E_v$ (kJ mol$^{-1}$) | 1.0[a] | 24.8 | 1.0[a] |
| $D_{MnH}^{298}$ ($10^{-10}$ m$^2$ s$^{-1}$) | 19.7 ± 2.6 | 23 | 26.9 |
| $E_{DMnH}$ (kJ mol$^{-1}$) | 33.0 ± 5.0 | 18 | 17.3 |
| $\Delta^2/10^{19}$ s$^{-2}$ | 3.7 ± 1.0 | 0.47 | 7.2 |
| $A_O/\hbar$ ($10^6$ rad s$^{-1}$) | −73.3 ± 0.6[d] | −32.7[d] | −46.0[d] |
| $r_{MnH}$ (Å) | 2.77[a] | 2.75[a] | 2.77[a] |
| $a_{MnH}$ (Å) | 3.6[a] | 3.2[a] | 3.6[a] |
| $q^{298}$ | 1 | 1 | 1 |

[a]Parameters fixed during the fitting procedure. [b]ref 14. [c]ref 61. [d]There has been some confusion about the sign of the $^{17}O$ isotropic in $Mn^{2+}$ complexes. The correct sign of $A_O/\hbar$ of a water molecule bound to $Mn^{2+}$ is negative and corresponds to negative spin densities at the point of the nucleus that causes an upfield shift of the $^{17}O$ NMR resonance.

The water exchange rate determined for $[Mn(nompa)(H_2O)]^+$ ($k_{ex}^{298} = 2.8 \times 10^9$ s$^{-1}$) is extremely fast, being ca. 6 times faster than in $[Mn(edta)(H_2O)]^{2-}$ ($k_{ex}^{298} = 4.7 \times 10^8$ s$^{-1}$)[18] and 2 orders of magnitude faster than in $[Mn(H_2O)_6]^{2+}$ ($k_{ex}^{298} = 2.8 \times 10^7$ s$^{-1}$).[15b] Although the water exchange rates determined for six- and seven-coordinated $Mn^{2+}$ complexes are generally faster than that of the fully aquated species, the water exchange rate determined for $[Mn(nompa)(H_2O)]^+$ represents one of the highest water exchange rates reported for a $Mn^{2+}$ complex. We attribute this fast water exchange rate to a low energy barrier between the six-coordinated ground state and the seven-coordinated transition state responsible for an associatively activated water exchange reaction. The fact that in the solid state the $[Mn(nompa)(H_2O)]^+$ is seven-coordinated appears to support this hypothesis.

The value obtained for the $^{17}O$ hyperfine coupling constant ($A_O/\hbar = -73.3 \pm 0.5 \times 10^6$ rads$^{-1}$) is considerably higher than that typically observed for $Mn^{2+}$ complexes ($-32 \times 10^6$ to $-43 \times 10^6$ rad·s$^{-1}$). A large value of the $^{17}O$ hyperfine coupling constant could also be related to a hydration number $q > 1$, but this is not consistent with the relaxivity data obtained for this compound. Our DFT calculations presented in the next section provide support to the unusually high $^{17}O$ hyperfine coupling constant obtained from the analysis of the $^{17}O$ NMR data.

**DFT Calculations.** The $Mn^{2+}$ complex of nompa$^-$ presents a dimeric structure in the solid state thanks to the formation of carboxylate bridges. However, the dimers present in the solid state are expected to dissociate in solution into the corresponding monomeric complexes.[14] For instance, [Mn(1,4-DO2A)] was found to exist in the solid state as a dimer due to the presence of bridging bidentate carboxylate groups ($\mu$–$\eta^1$-carboxylate),[64] but they break apart in solution with the concomitant entrance of a water molecule into the $Mn^{2+}$ coordination sphere.[18] The $\tau_R^{298}$ value obtained from the analysis of the $^1H$ NMRD profiles, which is very similar to those reported for small mononuclear $Mn^{2+}$ complexes, is in line with this hypothesis. Furthermore, the $^1H$ NMRD and $^{17}O$ NMR data clearly evidence the presence of only one water molecule coordinated to $Mn^{2+}$.

Previous work performed on $Gd^{3+}$ and $Mn^{2+}$ complexes with polyaminocarboxylate ligands showed that the explicit inclusion of at least two second-sphere water molecules is crucial for the computation of accurate distances between the metal ion and the oxygen atoms of coordinated water molecules as well as accurate $^{17}O$ $A_O/\hbar$ values.[15b,61,65] Geometry optimizations performed on the $[Mn(nompa)(H_2O)]^+ \cdot xH_2O$ systems ($x = 0$ or 2) at the TPSSh/SVP level show that the inclusion of two second-sphere water molecules decreases the Mn–$O_W$ distance from 2.275 to 2.188 Å. The optimized geometry of the $[Mn(nompa)(H_2O)]^+ \cdot 2H_2O$ system is shown in Figure 7,

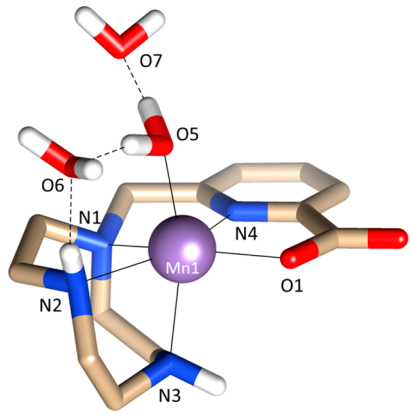


**Figure 7.** Geometry of the $[Mn(nompa)(H_2O)]^+ \cdot 2H_2O$ system optimized at the TPSSh/SVP level. Hydrogen atoms bound to carbon atoms are omitted for simplicity. Bond distances of the metal coordination environment: Mn1–O1, 2.133 Å; Mn1–N1, 2.439 Å; Mn1–N2, 2.306 Å; Mn1–N3, 2.311 Å; Mn1–O5, 2.188 Å. Hydrogen-bonding data: O5···O6, 2.730 Å; H5···O6, 1.761 Å; O5–H5···O6, 165.7°; N2···O6, 2.990 Å; H2···O6, 2.004 Å; N2–H2···O6, 159.9°; O5···O7, 2.706 Å; H5···O7, 1.717 Å; O5–H5···O7, 173.9°.

whereas optimized Cartesian coordinates are given in Tables S1 and S2 (Supporting Information). The two second-sphere water molecules are involved in hydrogen-bonding interaction with the coordinated water molecule, and one of them also with an NH group of the ligand. As expected, the metal is six-coordinated, being directly bound to the three nitrogen atoms of the tacn unit (Mn–N distances in the range of 2.30–2.44 Å), an oxygen atom of the carboxylate group (Mn–O distance = 2.133 Å), the nitrogen atom of the pyridyl unit, and the coordinated water molecule. These distances are in excellent agreement with those observed in the solid state for the enota complex, which show average Mn–O and Mn–N distances of 2.124 and 2.308 Å, respectively.[14] The coordination polyhedron around the $Mn^{2+}$ ion may be described as a distorted octahedron, where two of the nitrogen atoms of the tacn unit (N1 and N2), and the donor atoms of the picolinate moiety define one of the equatorial planes [mean deviation from planarity: 0.13 Å]. The *trans* angle O5–Mn1–N3 (162.4°) deviates by ca. 18° from the expected value for a regular octahedron (180°). Three of the *cis* angles of the equatorial plane are considerably smaller than the ideal value of 90° (71.3–75.5°), whereas the fourth *cis* angle of the equatorial plane is considerably larger [O1–Mn1–N2 137.7°]. The large value for the latter angle is probably responsible for the formation of the seven-coordinated species observed in the solid state for this complex.

The $^{17}O$ hyperfine coupling constant $A_O/\hbar$ was calculated on the $[Mn(nompa)(H_2O)]^+ \cdot 2H_2O$ system by following our


dx.doi.org/10.1021/ic500231z | Inorg. Chem. 2014, 53, 5136–5149

previously reported methodology (see the Computational Methods section above). Our calculations provide an $A_O/\hbar$ value of $-77.7 \times 10^6$ rad·s$^{-1}$, which corresponds to an $A_{iso}$ value of −12.36 MHz. This value is in excellent agreement with that obtained from the analysis of the $^{17}$O NMR data ($A_O/\hbar$ = $-73.3 \times 10^6$ rad·s$^{-1}$, −11.67 MHz). Two geometrical factors have been shown to affect considerably the $^{17}$O hyperfine coupling constant: the distance between the oxygen atom of the coordinated water molecule and the $Mn^{2+}$ ion, and the orientation of the water molecule plane with respect to the Mn−O vector.[15b,61] In the case of the $[Mn(nompa)(H_2O)]^+ \cdot 2H_2O$ complex, the calculated Mn1−O5 distance is rather short (2.188 Å), and the Mn1−O5−H−H angle (135°) is somewhat higher than the value obtained from analogous calculations for the $[Mn(edta)(H_2O)]^{2-}$ complex (115°). It is therefore probably responsible for the large $^{17}$O hyperfine coupling constant. Caravan at al. have recently developed an elegant method to estimate the hydration number of $Mn^{2+}$ complexes using $^{17}$O NMR line widths.[66] This method is valid as long as the hyperfine coupling constant $A_O/\hbar$ of the coordinated water molecule does not change significantly regardless of the other ligands coordinated to $Mn^{2+}$. The results reported here suggest that in some complexes $A_O/\hbar$ might vary significantly depending upon the nature of the complex. However, given the limited number of $Mn^{2+}$ complexes for which $A_O/\hbar$ has been determined, this has to be confirmed by enlarging the experimental data available in the literature.

The $^1$H hyperfine coupling constant obtained for $[Mn(nompa)(H_2O)]^+ \cdot 2H_2O$ ($A_H/\hbar = 4.8 \times 10^6$ rad·s$^{-1}$, 0.76 MHz) falls in between those obtained for $[Mn(H_2O)_6]^{2+}$ ($A_H/\hbar = 5.4 \times 10^6$ rad·s$^{-1}$)[15b] and $[Mn_2(enota)(H_2O)_2]$ ($A_H/\hbar = 2.9 \times 10^6$ rad·s$^{-1}$).[14] However, the fast electron spin relaxation of $[Mn(nompa)(H_2O)]^+$ and the very fast water exchange rate of the inner-sphere water molecule results in a negligible scalar contribution to relaxivity in spite of the sizable $A_H/\hbar$.[15b]

## CONCLUSIONS

Macrocyclic ligands Hnompa, Hdompa, and Htempa, which can be synthesized following very convenient routes, form thermodynamically stable $Mn^{2+}$ complexes in aqueous solutions. The stability constants are however more than 10 orders of magnitude lower than those of the corresponding $Cu^{2+}$ analogues. Furthermore, the kinetic inertness of the $Mn^{2+}$ complexes was found to be unsatisfactory for practical application as MRI contrast agents, which is related to the fast spontaneous dissociation of the complexes at pH 7.4. These results highlight the difficulties of designing thermodynamically stable and kinetically inert $Mn^{2+}$-based contrast agents, which remains a challenge for coordination chemists. The results presented in this paper also illustrate the difficulties associated with the prediction of the solution structure of $Mn^{2+}$ complexes with polyaminocarboxylates due to the symmetrical high-spin $d^5$ configuration of the metal ion. Indeed, the $Mn^{2+}$ complex of nompa$^-$ was found to be seven-coordinated in the solid state, but in solution the metal ion is six-coordinated by the pentadentate ligand and an inner-sphere water molecule. The complexes of tempa$^-$ and dompa$^-$ are six-coordinated and do not contain inner-sphere water molecules. The water exchange rate of the coordinated water molecule in $[Mn(nompa)(H_2O)]^+$ is extremely high, being 100 times faster than that of $[Mn(H_2O)_6]^{2+}$ and 6 times faster than that of $[Mn(edta)(H_2O)]^{2-}$. $^{17}$O NMR measurements and DFT calculations provide a very high $^{17}$O hyperfine coupling constant ($A_O/\hbar$ = $-73.3 \times 10^6$ rads$^{-1}$, −11.67 MHz as obtained from $^{17}$O NMR), which is about twice the value reported for $[Mn(H_2O)_6]^{2+}$ ($-34.6 \times 10^6$ rads$^{-1}$). These results indicate that caution should be taken when using $A_O/\hbar$ values for the estimation of hydration numbers of $Mn^{2+}$ complexes. The combined $^1$H NMRD, $^{17}$O NMR, and DFT approach reported here appears to be the most adequate to ensure a reliable estimation of the hydration number in $Mn^{2+}$ complexes.

## ASSOCIATED CONTENT

### Supporting Information

X-ray crystal structure of $[Mn_2(nompa)_2(H_2O)_2](ClO_4)_2$ in cif format, dependence of the pseudo-first-order rate constants on $Cu^{2+}$ ion concentration and the nature and the concentration of the buffers applied in the study, $^1$H NMR spectra and chemical shifts of Htempa recorded as a function of pH, temperature and pH dependence of $r_{1p}$ for $[Mn(nompa)(H_2O)]^+$, equations used for the analysis of the $^1$H NMRD and $^{17}$O NMR data, optimized Cartesian coordinates obtained with DFT calculations, potentiometric titration curves, absorption spectra of the $Cu^{2+}$−dompa system, pH-potentiometric titration curve of the $[Cu(dompa)]^+$ complex and additional pseudo-first-order rate constants obtained for the $[Mn(nompa)]^+$ complex (pseudo-first-order rate as a function of the nature and the concentration of the buffers applied in the study). This material is available free of charge via the Internet at http://pubs.acs.org.

## AUTHOR INFORMATION

### Corresponding Authors

*E-mail: carlos.platas.iglesias@udc.es.

*E-mail: gyula.tircso@science.unideb.hu.

### Notes

The authors declare no competing financial interest.

## ACKNOWLEDGMENTS

C.P.-I. is indebted to Centro de Supercomputación de Galicia (CESGA) for providing the computer facilities. E.M., G.T., F.K.K., and T.F. thank the Hungarian Scientific Research Fund (OTKA K-84291, and K-109029) and the TÁMOP-4.2.2.A-11/1/KONV-2012-0043 (ENVIKUT) project implemented through the New Hungary Development Plan, cofinanced by the European Social Fund and the European Regional Development Fund. This work was also supported by the János Bolyai Research Scholarship of the Hungarian Academy of Sciences. M.B. acknowledges support by the Compagnia di San Paolo through the project Nanoprogly (bando Ateneo-CSP). R.T., V.P., and N.C. acknowledge the French "Ministère de l'Enseignement Supérieur et de la Recherche" and the Centre National de la Recherche Scientifique (CNRS). This work has been carried out in the frame of the COST TD1004 "Theragnostics Imaging and Therapy: An Action to Develop Novel Nanosized Systems for Imaging-Guided Drug Delivery" Action.

## REFERENCES

(1) (a) Drahos, B.; Lukes, I.; Toth, E. *Eur. J. Inorg. Chem.* **2012**, 1975−1986. (b) Kueny-Stotz, M.; Garofalo, A.; Felder-Flesch, D. *Eur. J. Inorg. Chem.* **2012**, 1987−2005.

(2) (a) Dorazio, S. J.; Tsitovich, P. B.; Siters, K. E.; Spernyak, J. A.; Morrow, J. R. *J. Am. Chem. Soc.* **2011**, *133*, 14154−14156. (b) Dorazio, S. J.; Morrow, J. R. *Eur. J. Inorg. Chem.* **2012**, 2006−2014. (c) Dorazio, S. J.; Tsitovich, P. B.; Gardina, S. A.; Morrow, J. R. *J. Inorg. Biochem.* **2012**, *117*, 212−219.

(3) (a) Olantude, A. O.; Dorazio, S. J.; Spernyak, J. A.; Morrow, J. R. *J. Am. Chem. Soc.* **2012**, *134*, 18503−18505. (b) Dorazio, S. J.; Olantude, A. O.; Spernyak, J. A.; Morrow, J. R. *Chem. Commun.* **2013**, *49*, 10025−10027. (c) Tsitovich, P. B.; Spernyak, J. A.; Morrow, J. R. *Angew. Chem., Int. Ed.* **2013**, *52*, 13977−14000.
(4) Eisinger, J.; Shulman, R. G.; Blumberg, W. E. *Nature* **1961**, *192*, 963−964.
(5) Lauterbur, P. C. *Nature* **1973**, *242*, 190−191.
(6) (a) Zetter, M. S.; Grant, M.; Wood, E. J.; Dodgen, H. W.; Hunt, J. P. *Inorg. Chem.* **1972**, *11*, 2701−2706. (b) Koenig, S. H.; Baglin, C.; Brown, R. D., III; Brewer, C. F. *Magn. Reson. Med.* **1984**, *1*, 496−501. (c) Liu, G.; Dodgen, H. W.; Hunt, J. P. *Inorg. Chem.* **1977**, *16*, 2652−2653.
(7) Rocklage, S. M.; Cacheris, W. P.; Quay, S. C.; Hahn, F. E.; Raymond, K. N. *Inorg. Chem.* **1989**, *28*, 477−485.
(8) (a) Crossgrove, J.; Zheng, W. *NMR Biomed.* **2004**, *17*, 544−553. (b) Rivera-Mancía, S.; Ríos, C.; Montes, S. *Biometals* **2011**, *24*, 811−825.
(9) Tei, T.; Gugliotta, G.; Fekete, M.; Kálmán, F. K.; Botta, M. *Dalton Trans.* **2011**, *40*, 2025−2032.
(10) Jackels, S. C.; Durham, M. M.; Newton, J. E.; Henninger, T. C. *Inorg. Chem.* **1992**, *31*, 234−239.
(11) (a) Alexander, M. D.; Van Heuvelen, A.; Hamilton, H. G., Jr. *Inorg. Nucl. Chem. Lett.* **1970**, *6*, 445−448. (b) Drew, M. G. B.; bin Othman, A. H.; McFall, S. G.; Mcllroy, P. D. A.; Nelson, S. M. *J. Chem. Soc., Dalton Trans.* **1977**, 438−446. (c) Dabrowiak, J. C.; Nafie, L. A.; Bryan, P. S.; Torkelson, A. T. *Inorg. Chem.* **1977**, *16*, 540−544. (d) Newton, J. E.; Jackels, S. C. *J. Coord. Chem.* **1988**, *19*, 265−277.
(12) Drahos, B.; Kotek, J.; Hermann, P.; Lukes, I.; Toth, E. *Inorg. Chem.* **2010**, *49*, 3224−3238.
(13) Lieb, L.; Friedel, F. C.; Yawer, M.; Zahl, A.; Khusniyarov, M. M.; Heinemann, F. W.; Ivanović-Burmazović, I. *Inorg. Chem.* **2013**, *52*, 222−236.
(14) Balogh, E.; He, Z.; Hsieh, W.; Liu, S.; Toth, E. *Inorg. Chem.* **2007**, *46*, 238−250.
(15) (a) Ducommun, Y.; Newman, K. E.; Merbach, A. E. *Inorg. Chem.* **1980**, *19*, 3696−3703. (b) Esteban-Gomez, D.; Cassino, C.; Botta, M.; Platas-Iglesias, C. *RSC Adv.* **2014**, *4*, 7094−7103.
(16) (a) de Sá, A.; Bonnet, C. S.; Geraldes, C. F. G. C.; Tóth, E.; Ferreira, P. M. T.; André, J. P. *Dalton Trans.* **2013**, *42*, 4522−4532. (b) Drahoss, B.; Pniok, M.; Kotek, J.; Hermann, P.; Lukeš, I.; Tóth, E. *Dalton Trans.* **2011**, *40*, 10131−10146.
(17) Drahos, B.; Kotek, J.; Císarova, I.; Hermann, P.; Helm, L.; Lukes, I.; Tóth, E. *Inorg. Chem.* **2011**, *50*, 12785−12801.
(18) Rolla, G. A.; Platas-Iglesias, C.; Botta, M.; Tei, L.; Helm, L. *Inorg. Chem.* **2013**, *52*, 3268−3279.
(19) Kálmán, F. K.; Tircsó, G. *Inorg. Chem.* **2012**, *51*, 10065−10067.
(20) (a) Loving, G. S.; Mukherjee, S.; Caravan, P. *J. Am. Chem. Soc.* **2013**, *135*, 4620−4623. (b) Aime, S.; Botta, M.; Gianolio, E.; Terreno, E. *Angew. Chem., Int. Ed.* **2000**, *39*, 747−750.
(21) (a) Troughton, J. S.; Greenfield, M. T.; Greenwood, J. M.; Dumas, S.; Wiethoff, A. J.; Wang, J.; Spiller, M.; McMurry, T. J.; Caravan, P. *Inorg. Chem.* **2004**, *43*, 6313−6323. (b) Su, H.; Wu, C.; Zhu, J.; Miao, T.; Wang, D.; Xia, C.; Zhao, X.; Gong, Q.; Song, B.; Ai, H. *Dalton Trans.* **2012**, *41*, 14480−14483.
(22) (a) Rolla, G. A.; Tei, L.; Fekete, M.; Arena, F.; Gianolio, E.; Botta, M. *Bioorg. Med. Chem.* **2011**, *19*, 1115−1122. (b) Aime, S.; Anelli, P. L.; Botta, M.; Brochetta, M.; Canton, S.; Fedeli, F.; Gianolio, E.; Terreno, E. *Biol. Inorg. Chem.* **2002**, *7*, 58−67.
(23) Lima, L. M. P.; Esteban-Gomez, D.; Delgado, R.; Platas-Iglesias, C.; Tripier, R. *Inorg. Chem.* **2012**, *51*, 6916−6927.
(24) Frindel, M.; Camus, N.; Rauscher, A.; Bourgeois, M.; Alliot, C.; Barré, L.; Gestin, J.-F.; Tripier, R.; Faivre-Chauvet, A. *Nucl. Med. Biol.* **2014**, *21*, 418−423, DOI: 10.1016/j.arcped.2014.01.004.
(25) Mato-Iglesias, M.; Roca-Sabio, A.; Pálinkás, Z.; Esteban-Gómez, D.; Platas-Iglesias, C.; Tóth, É.; de Blas, A.; Rodríguez-Blas, T. *Inorg. Chem.* **2008**, *47*, 7840−7851.
(26) Irving, H. M.; Miles, M. G.; Pettit, L. *Anal. Chim. Acta* **1967**, *38*, 475−488.
(27) Zékány, L.; Nagypál, I. In *Computational Methods for Determination of Formation Constants*; Legett, D. J., Ed.; Plenum: New York, 1985; p 291.
(28) Corsi, D. M.; Platas-Iglesias, C.; van Bekkum, H.; Peters, J. A. *Magn. Reson. Chem.* **2001**, *39*, 723−726.
(29) *Crysalis Software System*, version 1.171.28 cycle4 beta; Oxford Diffraction Ltd.: Abingdon, U.K., 2005.
(30) SHELX Sheldrick, G. M. *Acta Crystallogr.* **2008**, *A64*, 112−122.
(31) Glasoe, P. K.; Long, F. A. *J. Phys. Chem.* **1960**, 188−189.
(32) Frisch, M. J.; Trucks, G. W.; Schlegel, H. B.; Scuseria, G. E.; Robb, M. A.; Cheeseman, J. R.; Scalmani, G.; Barone, V.; Mennucci, B.; Petersson, G. A.; Nakatsuji, H.; Caricato, M.; Li, X.; Hratchian, H. P.; Izmaylov, A. F.; Bloino, J.; Zheng, G.; Sonnenberg, J. L.; Hada, M.; Ehara, M.; Toyota, K.; Fukuda, R.; Hasegawa, J.; Ishida, M.; Nakajima, T.; Honda, Y.; Kitao, O.; Nakai, H.; Vreven, T.; Montgomery, Jr., J. A.; Peralta, J. E.; Ogliaro, F.; Bearpark, M.; Heyd, J. J.; Brothers, E.; Kudin, K. N.; Staroverov, V. N.; Kobayashi, R.; Normand, J.; Raghavachari, K.; Rendell, A.; Burant, J. C.; Iyengar, S. S.; Tomasi, J.; Cossi, M.; Rega, N.; Millam, N. J.; Klene, M.; Knox, J. E.; Cross, J. B.; Bakken, V.; Adamo, C.; Jaramillo, J.; Gomperts, R.; Stratmann, R. E.; Yazyev, O.; Austin, A. J.; Cammi, R.; Pomelli, C.; Ochterski, J. W.; Martin, R. L.; Morokuma, K.; Zakrzewski, V. G.; Voth, G. A.; Salvador, P.; Dannenberg, J. J.; Dapprich, S.; Daniels, A. D.; Farkas, Ö.; Foresman, J. B.; Ortiz, J. V.; Cioslowski, J.; Fox, D. J. *Gaussian 09*, revision B.01; Gaussian, Inc.: Wallingford CT, 2009.
(33) Tao, J. M.; Perdew, J. P.; Staroverov, V. N.; Scuseria, G. E. *Phys. Rev. Lett.* **2003**, *91*, 146401.
(34) Schaefer, A.; Horn, H.; Ahlrichs, R. *J. Chem. Phys.* **1992**, *97*, 2571−2577.
(35) Stanton, J. F.; Gauss, J. *Adv. Chem. Phys.* **2003**, *125*, 101−146.
(36) Montoya, A.; Truong, T. N.; Sarofim, A. F. *J. Phys. Chem. A* **2000**, *124*, 6108−6110.
(37) Rega, N.; Cossi, M.; Barone, V. J. *J. Chem. Phys.* **1996**, *105*, 11060−11067.
(38) Hedegard, E. D.; Kongsted, J.; Sauer, S. P. A. *J. Chem. Theory Comput.* **2011**, *7*, 4077−4087.
(39) Tomasi, J.; Mennucci, B.; Cammi, R. *Chem. Rev.* **2005**, *105*, 2999−3093.
(40) (a) Tjioe, L.; Joshi, T.; Forsyth, C. M.; Moubaraki, B.; Murray, K. S.; Brugger, J.; Graham, B.; Spiccia, L. *Inorg. Chem.* **2012**, *51*, 939−953. (b) Roger, M.; Patinec, V.; Bourgeois, M.; Tripier, R.; Triki, S.; Handel, H. *Tetrahedron* **2012**, *68*, 5637−5643. (c) Tjioe, L.; Meininger, A.; Joshi, T.; Spiccia, L.; Graham, B. *Inorg. Chem.* **2011**, *50*, 4327−4339. (d) Zhang, Q. F.; Yang, W. H.; Yi, W. J.; Zhang, J.; Ren, J.; Luo, T. Y.; Zhu, W.; Yu, X. Q. *Bioorg. Med. Chem. Lett.* **2011**, *21*, 7045−7049. (e) Chong, H.; Brechbiel, M. W. *Synth. Commun.* **2003**, *33*, 1147−1154. (f) Kimura, S.; Bill, E.; Bothe, E.; Weyhermuller, T.; Wieghardt, K. *J. Am. Chem. Soc.* **2001**, *123*, 6025−6039. (g) Kovacs, Z.; Sherry, D. A. *Tetrahedron Lett.* **1995**, *36*, 9269−9272. (h) Kruper, W. J.; Rudolf, P. R.; Langhoff, C. A. *J. Org. Chem.* **1993**, *58*, 3869−3876. (i) Van Westrenen, J.; Sherry, D. A. *Bioconjugate Chem.* **1992**, *3*, 524−532. (j) Sessler, J. L.; Sibert, J. W.; Lynch, V. *Inorg. Chem.* **1990**, *29*, 4143−4146.
(41) (a) Timmons, J. C.; Hubin, T. J. *Coord. Chem. Rev.* **2010**, *254*, 1661−1685. (b) Suchy, M.; Hudson, R. H. E. *Eur. J. Org. Chem.* **2008**, 4847−4865.
(42) (a) Roger, M.; Lima, L. M. P.; Frindel, M.; Platas-Iglesias, C.; Gestin, J. F.; Delgado, R.; Patinec, V.; Tripier, R. *Inorg. Chem.* **2013**, *57*, 5246−5259. (b) Gasser, G.; Tjioe, L.; Graham, B.; Belousoff, M. J.; Juran, S.; Walther, M.; Künstler, J. U.; Bergmann, R.; Stephan, H.; Spiccia, L. *Bioconjugate Chem.* **2008**, *19*, 719−730. (c) Stavila, V.; Allali, M.; Canaple, L.; Storzt, Y.; Franc, C.; Maurin, P.; Beuf, O.; Dufay, O.; Samarut, J.; Janier, M.; Hasserodt, J. *New J. Chem.* **2008**, *32*, 428−435.
(43) (a) Le Baccon, M.; Chuburu, F.; Toupet, L.; Handel, H.; Soibinet, M.; Déchamps-Olivier, I.; Barbier, J. P.; Aplincourt, M. *New J. Chem.* **2001**, *25*, 1168−1174. (b) Rohovec, J.; Gyepes, R.; Císařová, I.; Rudovský, J.; Lukeš, I. *Tetrahedron Lett.* **2000**, *41*, 1249−1253.

(44) (a) Le Baccon, M.; Chuburu, F.; Toupet, L.; Handel, H.; Soibinet, M.; Déchamps-Olivier, I.; Barbier, J. P.; Aplincourt, M. *New J. Chem.* **2001**, *25*, 1168−1174. (b) Rohovec, J.; Gyepes, R.; Císařová, I.; Rudovský, J.; Lukeš, I. *Tetrahedron Lett.* **2000**, *41*, 1249−1253.
(45) (a) El Hajj, F.; Patinec, V.; Triki, S.; Handel, H.; Marchivie, M. *Inorg. Chem. Commun.* **2010**, *13*, 1314−1316. (b) Bernier, N.; Tripier, R.; Patinec, V.; Le Baccon, M.; Handel, H. *C.R. Chimie* **2007**, *10*, 832−838. (c) Balogh, E.; Tripier, R.; Fousková, P.; Reviriego, F.; Handel, H.; Tóth, É. *Dalton Trans.* **2007**, 3572−3581. (d) Bernier, N.; Allali, M.; Tripier, R.; Conan, F.; Patinec, V.; Dévelay, S.; Le Baccon, M.; Handel, H. *New J. Chem.* **2006**, *30*, 435−441. (e) Dévelay, S.; Tripier, R.; Le Baccon, M.; Patinec, V.; Serratrice, G.; Handel, H. *Dalton Trans.* **2005**, 3016−3024.
(46) Belal, A.; Abdel-Rahman, L.; Amrallah, A. *J. Chem. Eng. Data* **1997**, *42*, 1075−1077.
(47) Riedo, T. J.; Kaden, T. A. *Helv. Chim. Acta* **1979**, *62*, 1089−1096.
(48) Hancock, R. D.; Shaikjee, M. S.; Dobson, S. M.; Boeyens, J. C. A. *Inorg. Chim. Acta* **1988**, *154*, 229−236.
(49) Motekaitis, R. J.; Rogers, B. E.; Reichert, D. E.; Martell, A. E.; Welch, M. J. *Inorg. Chem.* **1996**, *35*, 3821−3827.
(50) Xu, J.; Franklin, S. J.; Whisenhunt, D. W.; Raymond, K. N. *J. Am. Chem. Soc.* **1995**, *117*, 7245−7246.
(51) Margerum, D. W.; Cayley, G. R.; Weatherburn, D. C.; Pagenkopf, G. K. In *Coordination Chemistry*, Vol. 2; Martell, A. E., Ed.; American Chemical Society: Washington, DC, 1978, 1−220.
(52) Drahos, B.; Kubicek, V.; Bonnet, C. S.; Hermann, P.; Lukes, I.; Toth, E. *Dalton Trans.* **2011**, *40*, 1945−1951.
(53) Mahdi, M. M.; McKee, V. *Catal. Commun.* **2010**, *11*, 1032−1035.
(54) (a) Corey, E. J.; Bailar, J. C. *J. Am. Chem. Soc.* **1959**, *81*, 2620−2629. (b) Beattie, J. K. *Acc. Chem. Res.* **1971**, *4*, 253−259. (c) Notni, J.; Pohle, K.; Peters, J. A.; Gorls, H.; Platas-Iglesias, C. *Inorg. Chem.* **2009**, *48*, 3257−3267.
(55) Yang, Y.-S.; Gu, W.; Zhang, L.-Z.; Gao, F.-X.; Yan, S.-P. *J. Coord. Chem.* **2007**, *60*, 1913−1921.
(56) (a) Tei, L.; Bencini, A.; Blake, A. J.; Lippolis, V.; Perra, A.; Valtancoli, B.; Wilson, C.; Schroder, M. *Dalton Trans.* **2004**, 1934−1944. (b) Fukuda, Y.; Hirota, M.; Kon-no, M.; Nakao, A.; Umezawa, K. *Inorg. Chim. Acta* **2002**, *339*, 322−326.
(57) (a) Deng, D.; Liu, P.; Fu, W.; Long, L.; Yang, F.; Ji, B. *Inorg. Chim. Acta* **2010**, *363*, 891−898. (b) Du, Z.-X.; Li, J.-X. *Acta Crystallogr.* **2008**, *E64*, m1295−m1296.
(58) Casanova, D.; Alemany, P.; Bofill, J. M.; Alvarez, S. *Chem.—Eur. J.* **2003**, *9*, 1281−1295.
(59) Llunell, M.; Casanova, D.; Cirera, J.; Alemany, P.; Alvarez, S. *SHAPE*, program for the stereochemical analysis of molecular fragments by means of continuous shape measures and associated tools, version 2.1.
(60) (a) Pinsky, M.; Avnir, D. *Inorg. Chem.* **1998**, *37*, 5575−5582. (b) Casanova, D.; Cirera, J.; Llunell, M.; Alemany, P.; Avnir, D.; Alvarez, S. *J. Am. Chem. Soc.* **2004**, *126*, 1755−1763. (c) Cirera, J.; Ruiz, E.; Alvarez, S. *Chem.—Eur. J.* **2006**, *12*, 3162−3167.
(61) Patinec, V.; Rolla, G. A.; Botta, M.; Tripier, R.; Esteban-Gomez, D.; Platas-Iglesias, C. *Inorg. Chem.* **2013**, *52*, 11173−11184.
(62) Freed, J. H. *J. Chem. Phys.* **1978**, *68*, 4034−4037.
(63) Mills, R. *J. Phys. Chem.* **1973**, *77*, 685−688.
(64) Bianchi, A.; Calabi, L.; Giorgi, C.; Losi, P.; Mariani, P.; Palano, D.; Paoli, P.; Rossi, P.; Valtancoli, B. *J. Chem. Soc., Dalton Trans.* **2001**, 917−922.
(65) Esteban-Gomez, D.; de Blas, A.; Rodriguez-Blas, T.; Helm, L.; Platas-Iglesias, C. *ChemPhysChem* **2012**, *13*, 3640−3650.
(66) Gale, E. M.; Zhu, J.; Caravan, P. *J. Am. Chem. Soc.* **2013**, *135*, 18600−18608.